PROPELLER CHARACTERISTICS AND SLIPSTREAM EFFECTS ON A HIGH WING MONOPLANE FROM WIND TUNNEL TESTS.

BY

James Sargent Russell

PROPELLER CHARACTERISTICS AND SLIPSTREAM EFFECTS ON A HIGH WING MONOPLANE FROM WIND TUNNEL TESTS

Thesis by

J. S. Russell

and

H. M. McCoy

In partial fulfillment of the requirements for

the Degree of Master of Science in Aeronautical Engineering

California Institute of Technology
Pasadena, California
1935

PROPELLER CHARACTERISTICS AND SLIPSTREAM EFFECTS ON A HIGH WING MONOPLANE FROM WIND TUNNEL TESTS

Standard references on airplane propeller characteristics are N.A.C.A. Report # 350 (Weick) and N.A.C.A. Report # 491 (Hartman). With increased engine powers, modern types of cowling, increased number of blades, higher airplane speeds and greater engine-body diameters, there has been a growing need for investigation to extend the range of these references. While full scale data are desirable it is difficult to obtain them because of the limited capacity in size and airspeed in existing wind tunnels. The research herein reported was undertaken in order to examine the practicability of making propeller tests on a scale model in the wind tunnel.

The model was that of a representative high wing monoplane at one sixth scale. The model was complete except for landing gear and any protruding cockpit enclosures. The propeller diameter was 10/6 feet, the power was 432/36= 12 horse power, the rated maximum revolutions per minute were 12,000 so that the linear velocities of the blade elements were equal to those of a full scale propeller with rated maximum angular velocity of 2,000 R. P. M. Since the lengths of chord of blade were one sixth full scale the propeller was operating at a Reynold's Number of one sixth the Reynold's Number of the full scale propeller. The blade form was exactly that of a Hamilton Standard 1A1-0 propeller to one sixth scale.

The tests made fall into two classes.

1. Production of working charts to determine the propulsive efficiency of two and three bladed propellers at various blade angles, velocities and powers.
2. Investigation of the effect of slipstream on the performance and static longitudional stability of the airplane at various angles of climb and glide.

6394

Description of Apparatus

The principal advantages of a powered model test over a full scale flight test are ease of control and facility in measuring the forces and moments developed In the wind tunnel, power output results are read on the external balance system as in a normal wind tunnel test. The G.A.L.C.I.T. six component system is shown in Figure 1. Here, air velocity, geometrical angle of attack, thrust, drag, lift and moments are measured. The measurement of power input is more complicated and is accomplished by means of a revolution counter and a torque meter.

The revolution counting system, or timing circuit, shown in Figure 3, consists of a pendulum actuated, multiple relay circuit which counts the motor revolutions over an accurate time interval of about ten seconds. The timing system was calibrated for each run against a crystal controlled accurate fifty cycle current.

The location and functioning of the torque meter is shown diagrammatically in Figure 2. The adjoining sketch shows the arrangement, used in the experiment, of an alternating current Wheatstone Bridge for indicating torque. The torque being developed by the propeller is opposed in equal amount by the resisting moment in twist developed by the torque bar. The angle of twist varies the position of the soft iron armature between the pole faces of coils (1) and (2), thus varying their impedance. The relative change in impedance is indicated in balancing the Bridge by means of the variable resistance. The reading of the variable resistance of the Wheatstone Bridge, in ohms, is converted to torque, in kilogram-meters, by means of a calibration curve constructed for each run. This curve represents the mean of calibrations made before and after the run. The calibration is made by keying a bar of fifty

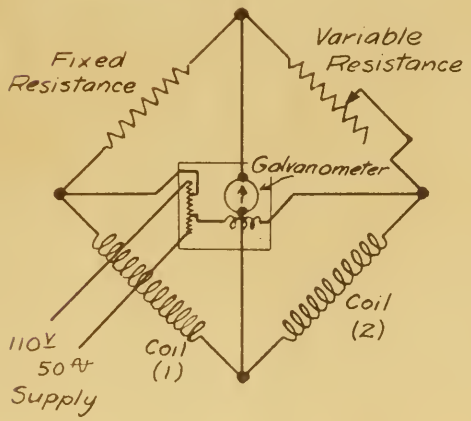

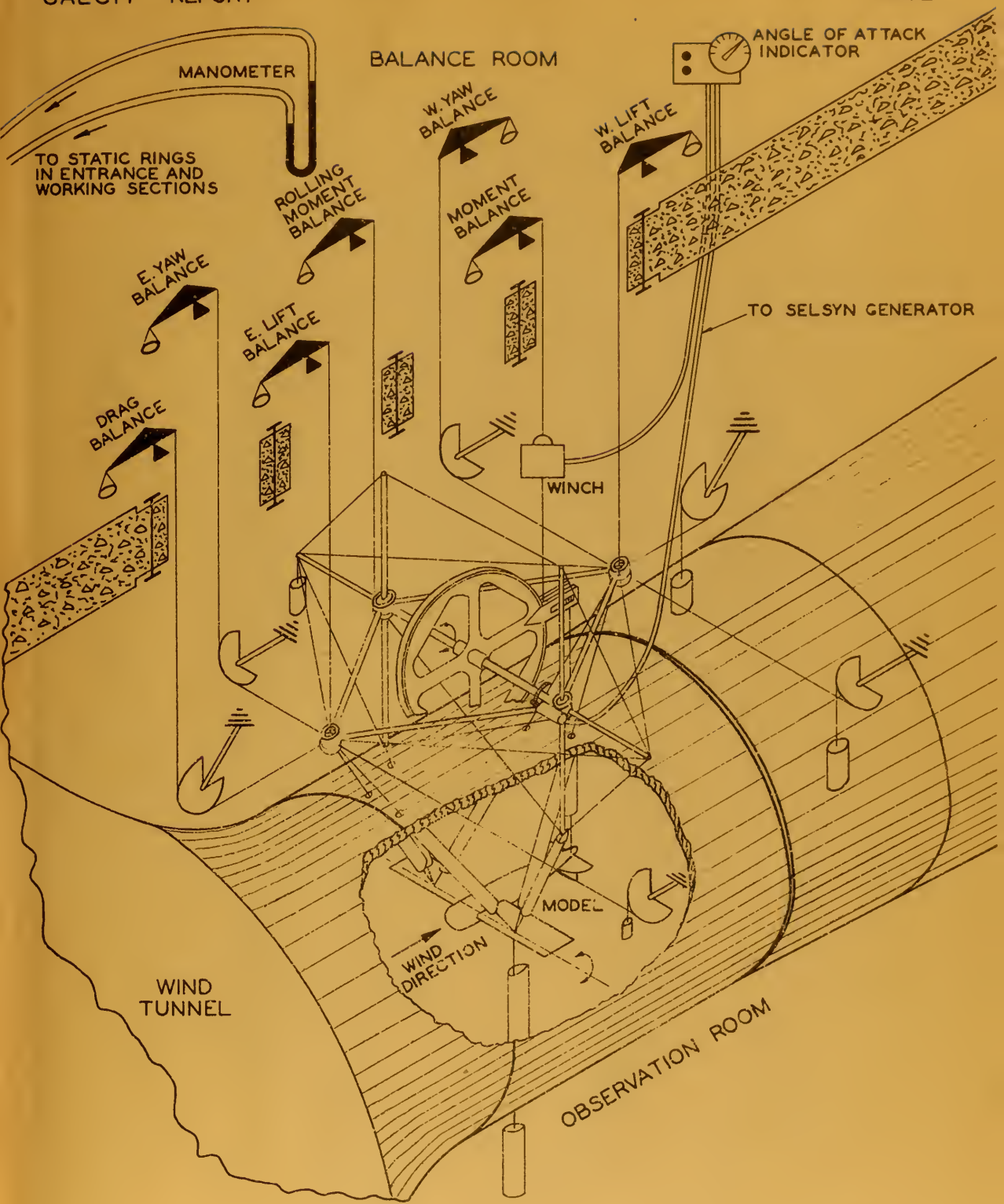

SIX COMPONENT SETUP FOR TEN FOOT WIND TUNNEL TESTS
AT GUGGENHEIM AERONAUTICS LABORATORY
CALIFORNIA INSTITUTE OF TECHNOLOGY

FIG. 1.

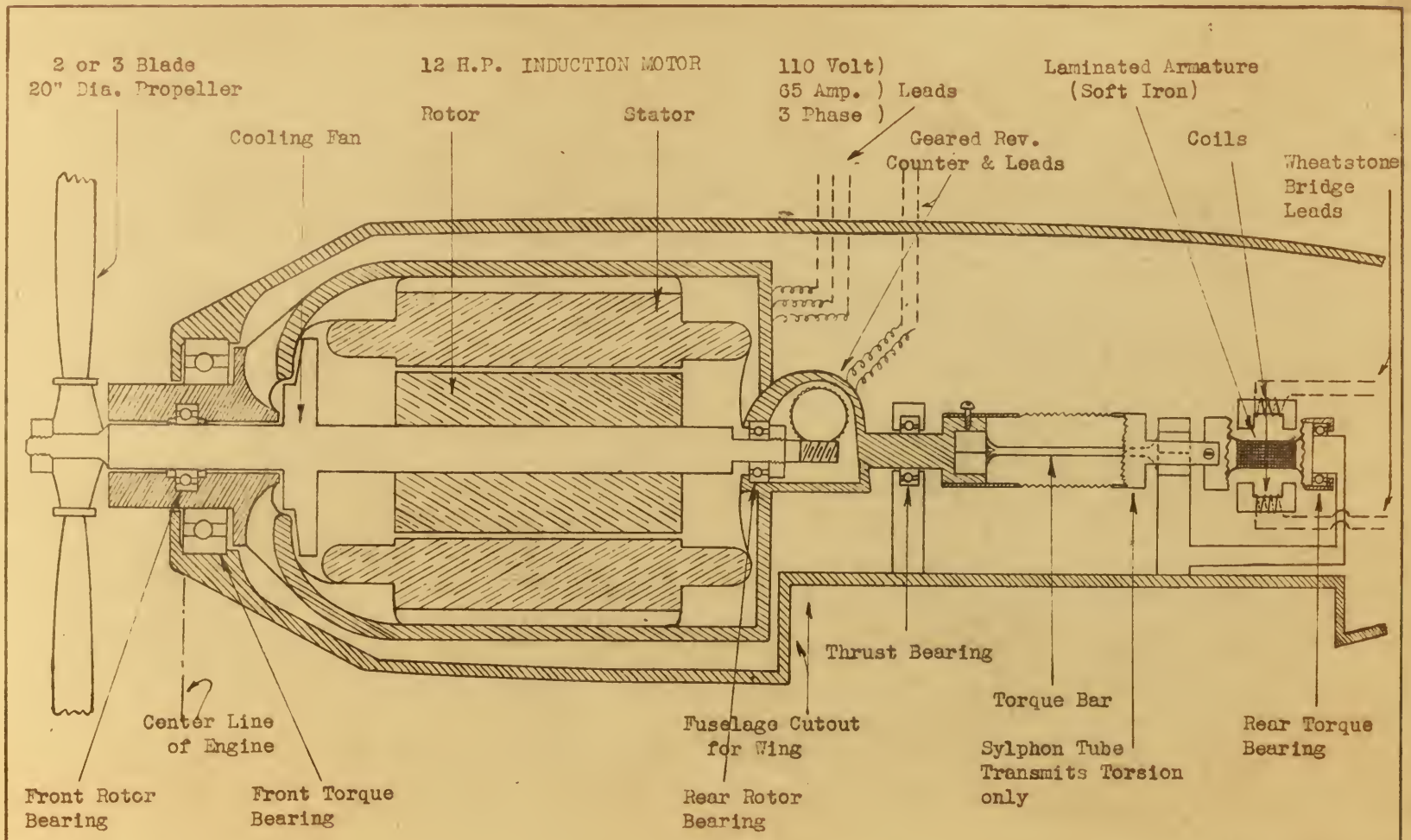

SCHEMATIC DIAGRAM OF POWER PLANT MODEL

FIGURE 2

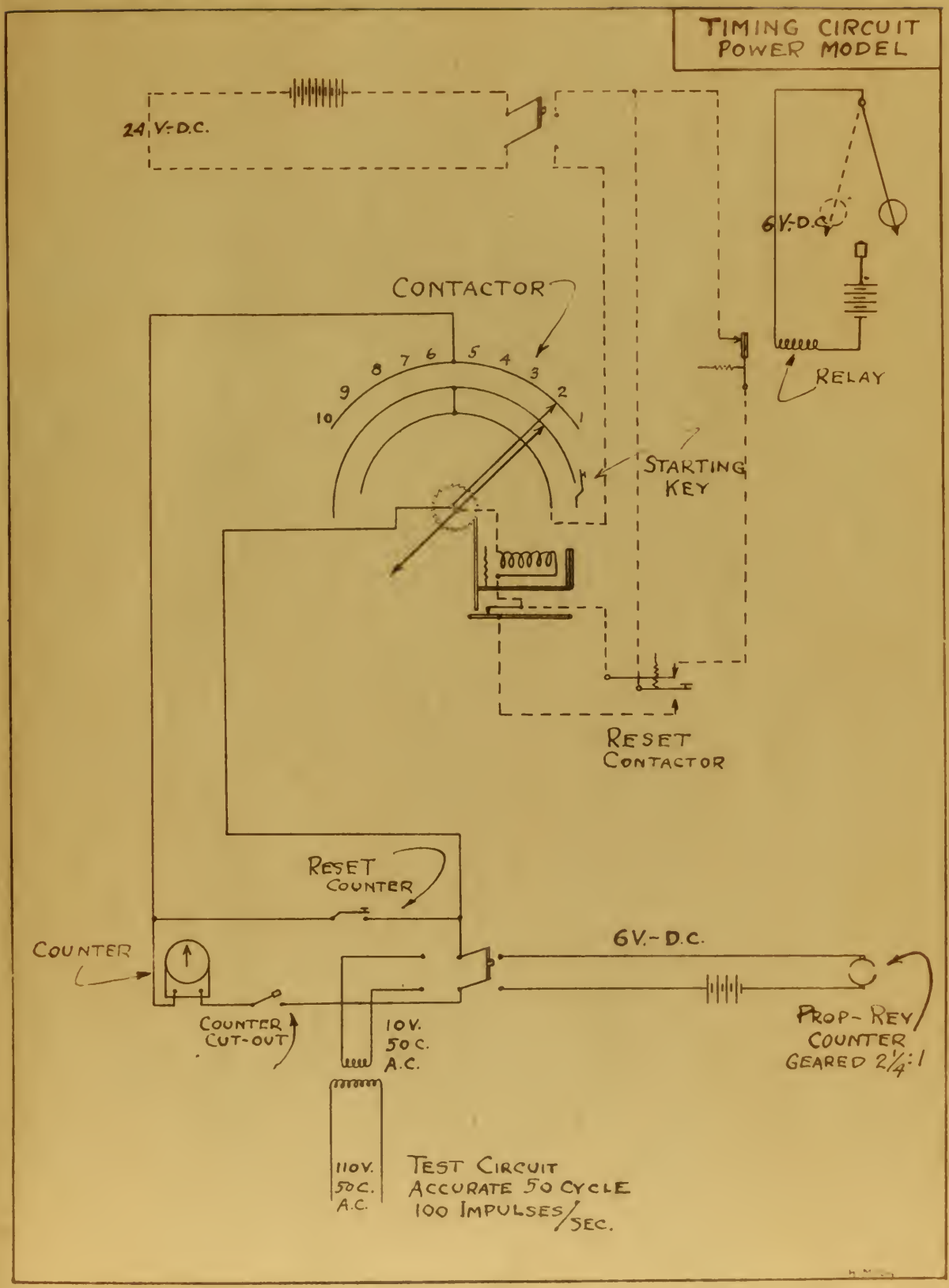
TIMING CIRCUIT
POWER MODEL
24 V-D.C.
6 V.-D.C.
CONTACTOR
10
9
8
7
6
5
4
3
2
1
RELAY
STARTING KEY
RESET CONTACTOR
RESET COUNTER
COUNTER
6V.-D.C.
COUNTER CUT-OUT
10V. 50 C. A.C.
PROP-REY COUNTER GEARED 2¼:1
110V. 50C. A.C.
TEST CIRCUIT ACCURATE 50 CYCLE 100 IMPULSES/SEC.

FIGURE 3

centimeters length to the stator and placing known weights in pans suspended from knife edges at each end. In this manner a known torque is given in terms of resistance reading.

Photographs, Figure 4., show views of the model, instrument table, parts and torque calibration arrangement.

MODEL DISASSEMBLED

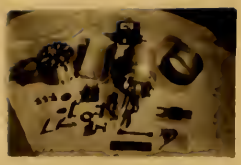

MOTOR & MODEL PARTS

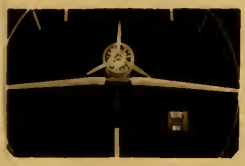

FRONT VIEW

THREE QUARTER VIEW

SIDE VIEW

SIDE VIEW

TORQUE CALIBRATION

INSTRUMENT TABLE

FIGURE 4.

PART ONE

PROPELLERS

The first problem of the investigation was the determination of the characteristics of two and three bladed propellers. A plot of initial data obtained from two bladed propellers, when compared with the full scale data recorded by Weick in N.A.C.A. Technical Report #350, indicated sufficient agreement between model and full scale characteristics to warrant complete tests.

If air were an incompressible fluid, if a degree of turbulence existed in the wind tunnel which was exactly that of the air in which the full scale airplane was to fly, if propellers were made of infinitely rigid material of absolutely smooth surface then we might expect to get results from wind tunnel tests which were fairly representative of geometrically similar full scale propellers. Fairly representative because there remains an element of uncertainty as to the effect of the presence of the wind tunnel walls on the flow through the propeller.

An enumeration of the factors wherein differences between model and full scale propeller characteristics might arise which we have considered are:-

1. Scale or Reynold's Number, roughness, turbulence.
2. Blade deflection.
3. Tip losses - compressibility.
4. Wind tunnel wall interference.
5. Experimental error.

Keeping these factors in mind let us consider the method of working up the data obtained. Lift, drag, and pitching moments were measured in the standard way by direct measurement of the forces transmitted through the model rigging to the automatic balances. Torque developed in the propeller shaft was recorded by a remote reading dynamometer. The revolutions of the propeller were obtained by direct count over a time interval.

The indicated drag-wise force, in the case of power-on, is transmuted into a combination of thrust and drag. It is apparent that the presence of the slip-stream over the model must cause some change in drag. This small change in drag is nicely disposed of by including it algebraically in the effective thrust. If we take the difference between the drag reading power-on, R, and the ordinary drag of the model with the propeller off, D_o, there remains a force which we can call effective thrust,-i.e. the true thrust minus the increment in drag due to the propeller slip-stream acting over the model

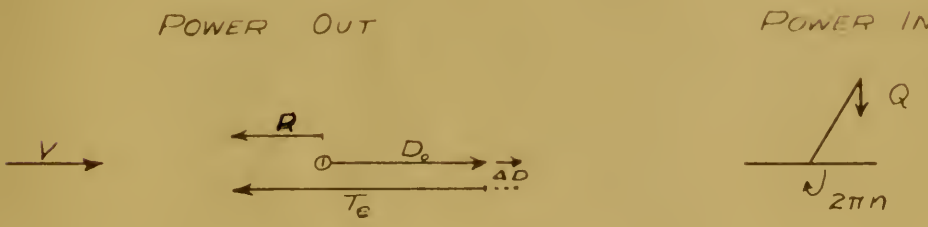

T_e x V is then the effective thrust horse power being developed by the propeller. Against this power output is the power input represented by the torque "Q", multiplied by the rotational velocity "2πn". Efficiency is the ratio of power out to power in - i.e. $\frac{T_e V}{2\pi n Q} = \eta$

It is convenient to put thrust, torque, and velocity into dimensionless coefficients. Since the velocity in the wind tunnel is recorded in combination with air density as the dynamic pressure being developed in the working section, the form $T = T_c \rho V^2 D^2$ is suggested, which can be written $T = T_c 2qD^2$. Likewise for torque, $Q = Q_c 2qD^3$. Velocity must be considered in the advance ratio of the propeller, $= \frac{V}{nD}$. The wind tunnel sensitive manometer records $\frac{\rho V^2}{2}$ by calibration against a pitot tube traverse of the working section of the tunnel. Velocity can be obtained from $V = \sqrt{2q/\rho}$ where ρ, air density, is a function of temperature and humidity of the air stream, barometric pressure, and gravity at the wind tunnel. η can be gotten directly from T_c and Q_c :-

$$\eta = \frac{T_c V}{P} = \frac{T_c 2q D^2 V}{2\pi n Q_c 2q D^3} = \frac{1}{2\pi}\,\frac{T_c}{Q_c}\,J \qquad \text{where } J = \frac{V}{nD}$$

C_s from $$C_s = \frac{\rho^{\frac{1}{5}} V}{n^{\frac{2}{5}} P^{\frac{1}{5}}} = \frac{\rho^{\frac{1}{5}} V}{2\pi n^{\frac{3}{5}} Q_c^{\frac{1}{5}} \rho^{\frac{1}{5}} V^{\frac{2}{5}} D^{\frac{3}{5}}} = \frac{1}{2\pi}\left(\frac{V}{nD}\right)^{\frac{3}{5}} \frac{1}{Q_c^{\frac{1}{5}}} = \frac{1}{2\pi}\,\frac{J^{\frac{3}{5}}}{Q_c^{\frac{1}{5}}}$$

C_T and C_Q, which are sometimes convenient, are simply $T_c J^2$ and $Q_c J^2$. Hartman's coefficients C_{QS} and $\frac{C_T}{C_Q}$ come out simply as $\frac{1}{\sqrt{Q_c}}$ and $\frac{T_c}{Q_c}$.

When the experiment was begun it was the opinion that some kind of preliminary fairing would be essential in order to get smooth final curves. Therefore T_c and Q_c were plotted against J, and points taken at even increments of J to solve for η and C_s. While this method produced smooth curves a very small displacement of the fairing caused comparatively large variations in peak efficiencies (1 - 2%). This method was discarded in favor of making a complete calculation for every experimental point and plotting the point without preliminary fairing on the final curve sheet (cf. Fig. 5). This direct plotting of unfaired results was followed in every case except that of the three low blade angles of the two bladed propeller where it was necessary, due to blade deflection and tip loss, to fair η against J before the final plot.

Having indicated the manner in which the propeller charts were made up let us return to a consideration of those factors which might affect extrapolation to full scale.

Reynold's Number: The actual velocities of the blade elements were made equal to those of full scale by increasing the rotational velocity of the propeller six times (2,000 r.p.m. full scale vs. 12,000 r.p.m. model). Axial wind velocities of 200 m.p.h. and upwards are obtainable in the California Institute of Technology wind tunnel, hence the airspeed of full scale flight could be used. The irreparable difference in Reynold's Number lay in the characteristic length, which of necessity remained at one sixth full scale. It should be noted that if the length of chord be used for the characteristic length, the Reynold's Number of even a full scale propeller element is small compared to the Reynold's Number of a full scale airfoil section as used in a wing. Research in the


C_s
1.0
1.5
2.0
2.5
16°
18°
20°
24°
28°
32°
3 Bladed Propeller 20 inch Diameter
⅙ Scale Model with Fuselage, High Wing, Vertical & Horizontal Tail Surfaces, N.A.C.A. Engine Cowl, & Tail Wheel
Plot of Original Experimental Points
Radius


3 Bladed Propeller 20 inch Diameter
1/6 Scale Model with Fuselage, High Wing, Vertical & Horizontal Tail Surfaces, N.A.C.A. Engine Cowl, & Tail Wheel
Plot of Original Experimental Points
12°
16°
20°
24°
28°
32°
Line of Max. η for C_s
C_s

There results a couple tending to raise the entering edge of the blade. The strength of this couple varies approximately with the square of the air velocity over the blade element and linearly with its effective angle of attack.

Tip Loss:- Inextricably bound up with blade deflection in our experimental data is tip loss. Our tip speeds were those of full scale. Both British and American experiments have shown, however, that at high tip speeds scale effect will be more strongly in evidence than at lower speeds.

The plot of points for 12°, 16°, and 20° blade angles, two bladed propeller, showed effects of tip speed and blade deflection. A special study was made of these conditions for the 16° blade setting and is presented in Figures 6 & 7. The 16° blade setting was chosen because the greatest variations in power and tip speed were obtained with this setting and the recorded data could be compared with a lower setting, 12°, and a higher setting 20°. It is to be noticed that only these three lowest settings for the two bladed propeller gave such variations in experimental data as to require fairing independent from the final plot. the three bladed propeller, having one additional blade lending its quota of work to provide a given thrust, showed insufficient scatter of points even at the lowest blade setting to warrant preliminary fairing.

Returning to Figures 6 & 7, it can be seen that under the higher power loadings the characteristic curves of the propeller move over in the direction to join the family of curves of the next higher blade setting. If one scales off the shift of the curve T_c vs J in Figure 6, against the main interval between curves, 4°, an indication is given of the effective twist of the blade in terms of blade setting at the .75 radius. As the tip speed increases, however, the effect of increase of blade angle is gradually overcome by tip loss and the curve drops back again, to or beyond, the curve obtained from lower power loading.

The question arises as to how the fairing of η vs J curves of Figure 7. shall be carried out under such circumstances in order to represent practically the efficiency of the propeller at the given blade angle. The method actually used was something of a compromise. Below the peak efficiency (and the region

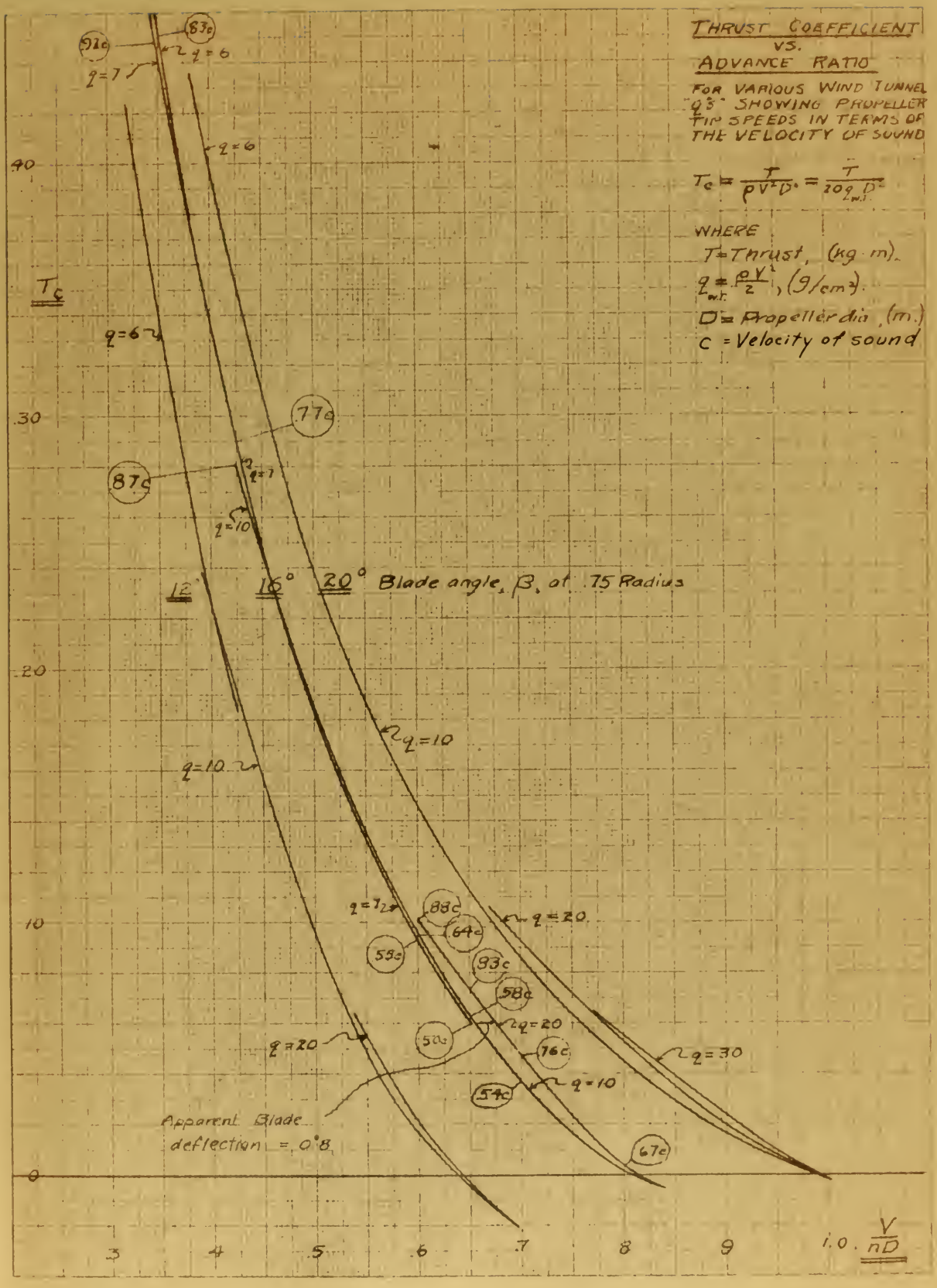
THRUST COEFFICIENT
VS.
ADVANCE RATIO
FOR VARIOUS WIND TUNNEL
Q's SHOWING PROPELLER
TIP SPEEDS IN TERMS OF
THE VELOCITY OF SOUND
$T_c = \frac{T}{\rho V^2 D^2} = \frac{T}{2 q_{wt} D^2}$
WHERE
T = Thrust, (kg m).
$q_{wt} = \frac{\rho V^2}{2}$, (g/cm²).
D = Propeller dia, (m.)
c = Velocity of sound
T_c
.40
.30
.20
10
0
91c
83c
87c
77c
88c
64c
59c
93c
58c
50c
76c
54c
67c
q=7
q=6
q=10
q=20
q=30
12°
16°
20° Blade angle, β, at .75 Radius
Apparent Blade deflection = 0°8
3
4
.5
.6
.7
8
9
i.o. $\frac{V}{nD}$

FIGURE 6

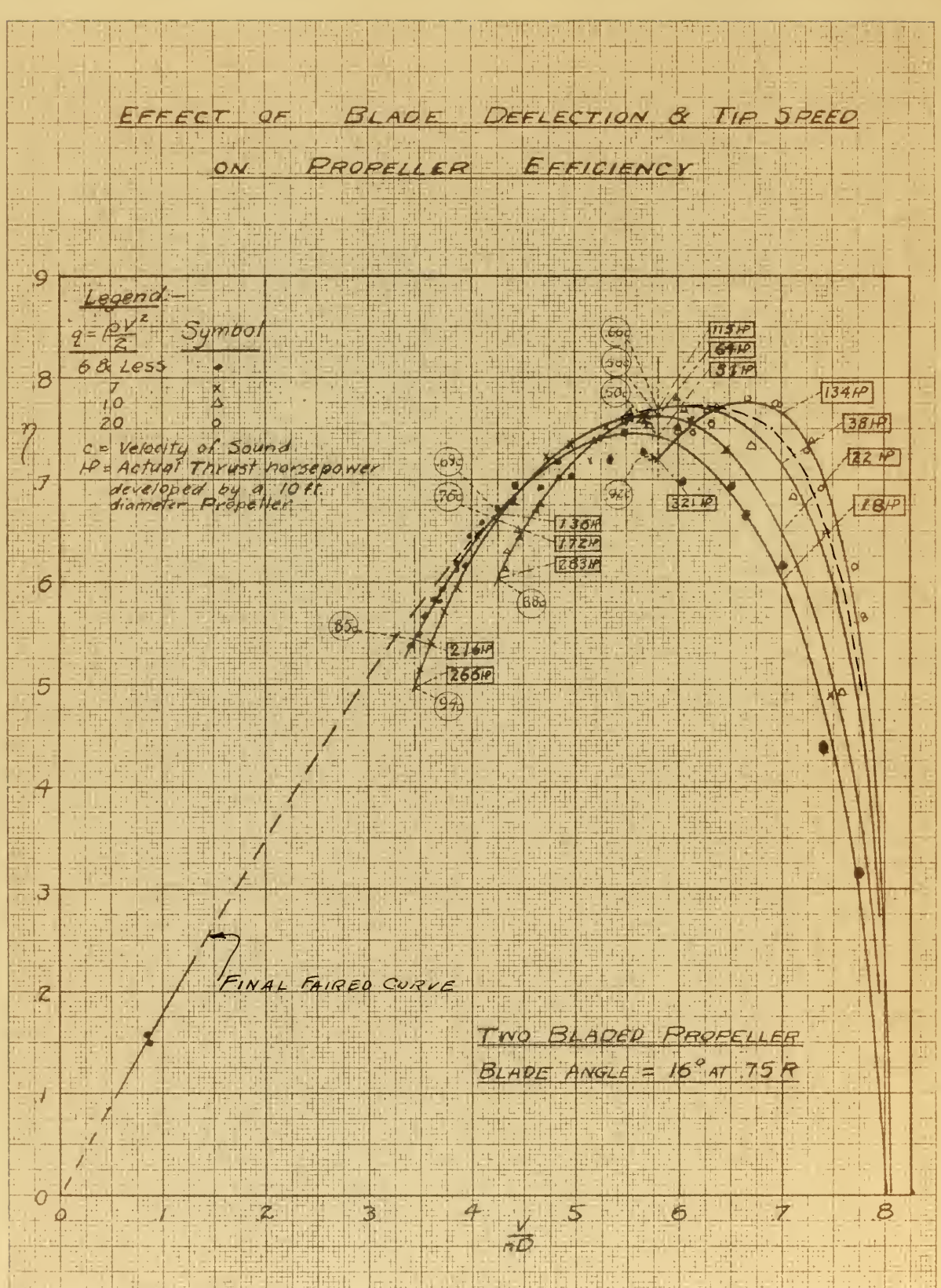
EFFECT OF BLADE DEFLECTION & TIP SPEED
ON PROPELLER EFFICIENCY
Legend –
$q = \frac{\rho V^2}{2}$ Symbol
6 & Less
7
10
20
C = Velocity of Sound
HP = Actual Thrust horsepower developed by a 10 ft. diameter Propeller
69q
76q
85q
88q
94q
66q
56q
50q
92q
115 HP
64 HP
51 HP
134 HP
38 HP
22 HP
18 HP
321 HP
136 HP
172 HP
283 HP
216 HP
266 HP
FINAL FAIRED CURVE
TWO BLADED PROPELLER
BLADE ANGLE = 16° AT .75 R
η
0
1
2
3
4
5
6
7
8
9
$\frac{V}{nD}$

FIGURE 7

in which the propeller would ordinarily be working) the envelope of the curves was taken. Reich has worked up a very comprehensive and complete set of data on the correction of propulsive efficiency for tip speed. The envelope of efficiency curves is our best estimate of the efficiency of the propeller without tip loss. A point taken from the curve then in this region may be corrected for tip loss using Reich's full scale results in this connection.

The region to the right of the peak and the peak itself present a greater problem. Reasonably the lower power loadings could be used and a correction applied for power (that is- blade deflection due to power loading), but lower power means lower forces actually measured and at small forces our experimental accuracy falls off. Hence the writers took arbitrarily a [redacted] mean of the points at the peak efficiency and beyond as being the best representation of the actual characteristics of the propeller at the given blade setting. The final faired curve used in presenting the [redacted] data is shown dotted in Figure 7.

Wind Tunnel Wall Interference:-

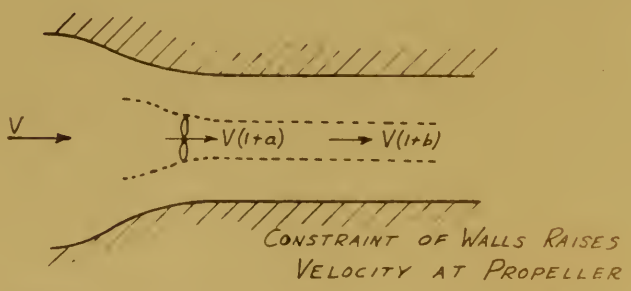

A glance at the sketch will indicate that free air conditions do not exist in the wind tunnel, but that constriction of the walls on the flow give a somewhat higher effective velocity to the air in which the propeller is working when compared to that velocity were the propeller operating in free air. Glauert (in R. & M. 1566) has developed a fairly accurate approximate formula for this increase in velocity. Glauert's formula has been used to compute a correction for wind tunnel wall interference applicable to our conditions. Figure 8. shows this correction in terms of the thrust coefficient T_c ; Figure 9. shows the range of T_c used in the experiment. It is evident that this correction can be safely neglected as it is well within the experimental error.

WIND TUNNEL INTERFERENCE EFFECT ON A MODEL PROPELLER FOR A CLOSED CIRCULAR THROAT & RATIO THROAT DIA / PROPELLER DIA. = 6/1

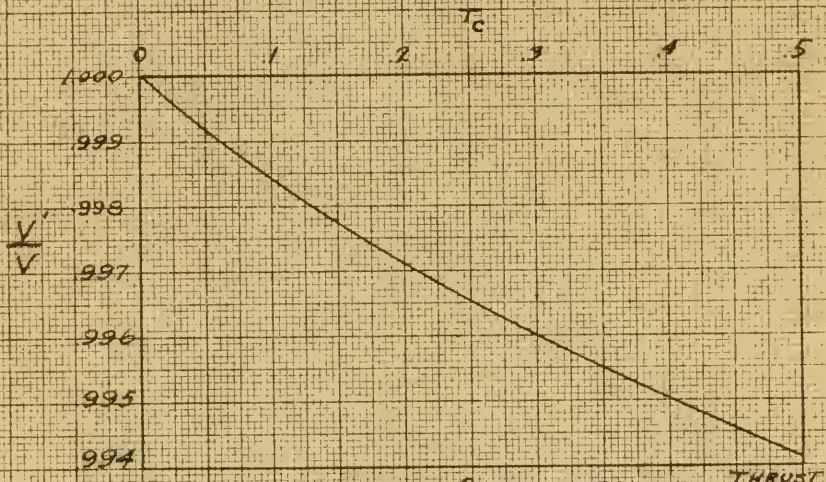

T_c = THRUST COEFFICIENT = $\frac{\text{THRUST}}{\rho V^2 D^2}$

V' = FREE AIR VELOCITY

V = WIND TUNNEL AIR VELOCITY

ρ = AIR DENSITY

D = DIAMETER OF PROPELLER

$$\frac{V'}{V} = 1 - \frac{\tau \alpha}{2\sqrt{1+2\tau}}, \qquad \tau = \frac{\text{THRUST}}{A \rho V^2}, \qquad \alpha = \frac{A}{C}$$

A = PROPELLER DISC AREA

C = WIND TUNNEL THROAT AREA

(Reference R & M 1566)

FIGURE 8

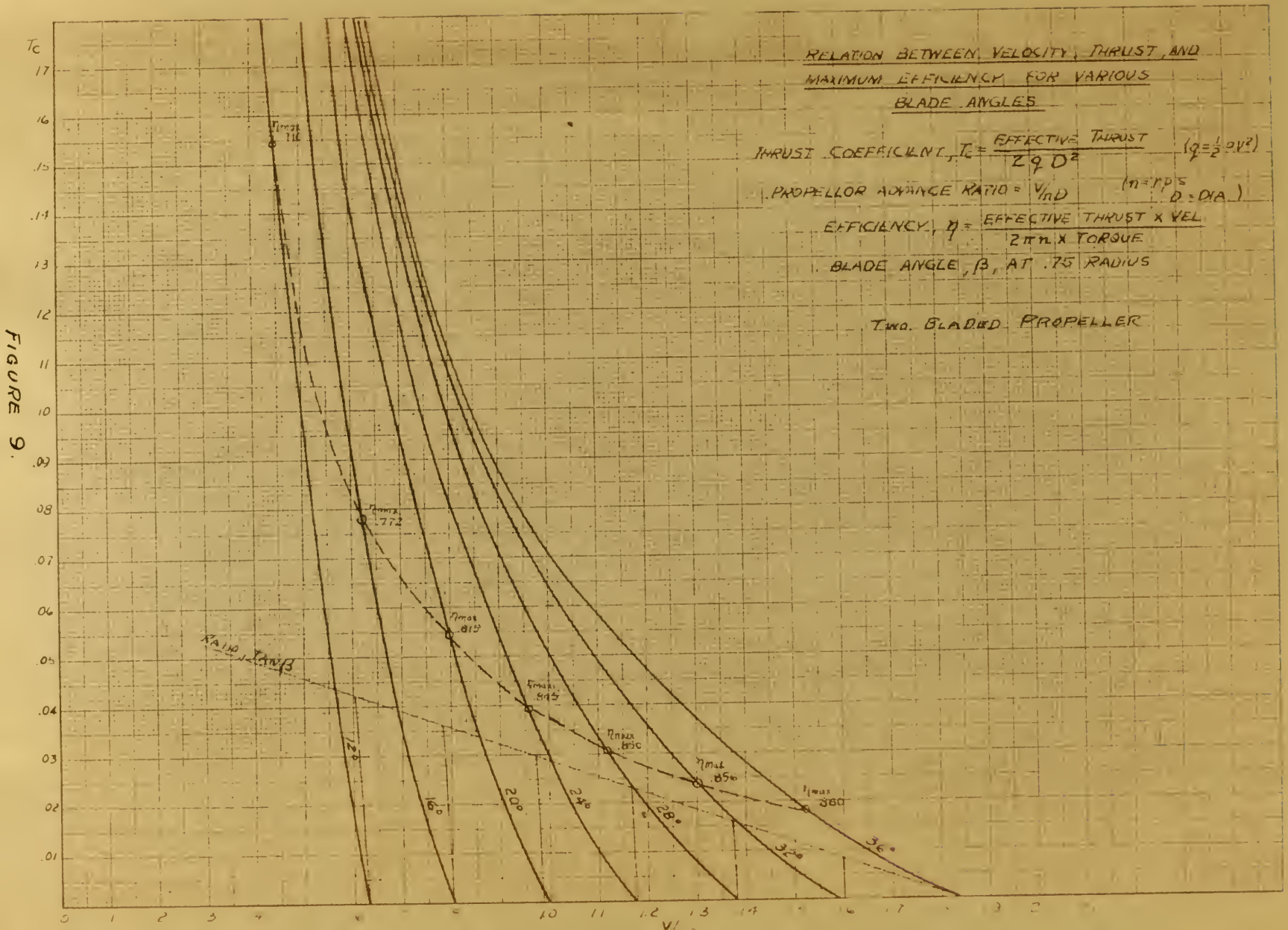
RELATION BETWEEN VELOCITY, THRUST, AND MAXIMUM EFFICIENCY FOR VARIOUS BLADE ANGLES
THRUST COEFFICIENT, $T_c = \frac{\text{EFFECTIVE THRUST}}{2\rho D^2}$ $(q = \frac{1}{2}\rho V^2)$
PROPELLOR ADVANCE RATIO = V/nD $(n = rps$ $D = DIA.)$
EFFICIENCY, $\eta = \frac{\text{EFFECTIVE THRUST} \times \text{VEL}}{2\pi n \times \text{TORQUE}}$
BLADE ANGLE, β, AT .75 RADIUS
TWO BLADED PROPELLER
T_c
V/nD
RATIO η max to β
ηmax .772
ηmax .815
ηmax .845
ηmax .850
ηmax .860
ηmax .880
12°
16°
20°
24°
28°
32°
36°

FIGURE 9.

Experimental Errors

Quantity	Range of Measurement	Probable Error
Lift, drag	0 - 600 Kg.	~~.002~~ 00.2 %
Torque, Q	-.2 to + .7 Kg. M.	.005 kg.-M.
Blade angle	12° to 36°	$0^{\circ}.1$
Revolutions/sec.,n	50 to 250 r.p.s.	0.2 r.p.s.

Every effort was made to represent accurately the actual quantities measured.

Discussion of Propeller Data:-

It must be noted that with the model's thrust line horizontal the propeller was acting in front of a wing at a $C_L = 0.3$. Assuming elliptical lift distribution , (with no distortion due to slipstream), and an upwash at the propeller ahead of the wing equal to .75 of the downwash at the wing, (the value of .75 was estimated from Glauert's " Aerofoil and Airscrew Theory" page 162), it can be seen that the propeller was acting in an upwash of $.75\frac{C_L}{\pi AR} \times 57.3 = 0^{\circ}.68$ This corresponds to about a cruising attitude, level flight, for the normal airplane.

It must be noted also that the full length blade was used whereas in practice the blade usually has some of the tip length removed. Figure 10. shows the principal characteristics of the blade used.

Figures 11. & 12. are two and three bladed propeller, basic working charts as obtained from our obervations. It must be emphasized that in computing C_s for entering the three bladed propeller chart(Figure 12.) that full power should be used.

Figures 13. - 18. present various comparisons of the data obtained.

In order to ascertain the appropriateness of applying the model data to full scale propellers a considerable amount of data on full scale propeller settings was obtained. The writers are indebted to the various airplane manufacturing concerns for their kind and helpful cooperation in this study. When worked up and plotted on the propeller characteristic charts, the $\frac{V}{nD}$ vs C_s

points group surprisingly well along the line of best efficiency as determined by the model tests (cf. Figures 13 & 14). The blade angles differ considerably from those of the model propeller but this may be expected from the differences in blade design and the amount of the tip of the blade removed to meet design conditions. The flight test data (cf. Tables 1 - 3) are included in this paper because they were carefully compiled and should furnish good design information. It should be noted that blade angles, β, are taken at the 42" station in many cases instead of at the .75 radius as was done in the model experiment.

A study of the flight test data and comparison with Figures 13 & 14 will show that many of the points are special cases. Examples are two pitch propellers at low pitch, and the same at high pitch where the propeller blade angle has been given full throw against a stop.

Figure 15 compares the C.A.L.C.I.T. two bladed propeller results with those obtained by the N.A.C.A. The comparison is made with the data from Fuselage 6, (Figure 14), of N.A.C.A. Report # 350, which resembled our configuration better than any of the other configurations used by the N.A.C.A. in that it had a completely cowled engine. Unfortunately the fuselage is rectangular in cross section and wing and tail surfaces are absent. The lower envelope of efficiency curves from the C.A.L.C.I.T. data can be attributed, in the writers' opinion, to the presence of the wing, to different shape and relative size of fuselage, and to scale effect. In Figure 16, (comparison of two and three bladed characteristics), it is interesting to note that differences are not so great as has been generally assumed.

Figure 17 shows that Weick's recommended 70% power absorption by a three bladed propeller as against a two bladed propeller is a good average assumption, but that at higher advance ratios the three bladed is operating under improving conditions.

Figure 18 compares C.A.L.C.I.T. and N.A.C.A. curves (fuselage 6 Figure 14 Report #350) of Blade Angles vs C_s directly.

BLADE FORM CURVES

FOR TWO & THREE BLADED PROPELLERS

USED IN MODEL TESTS

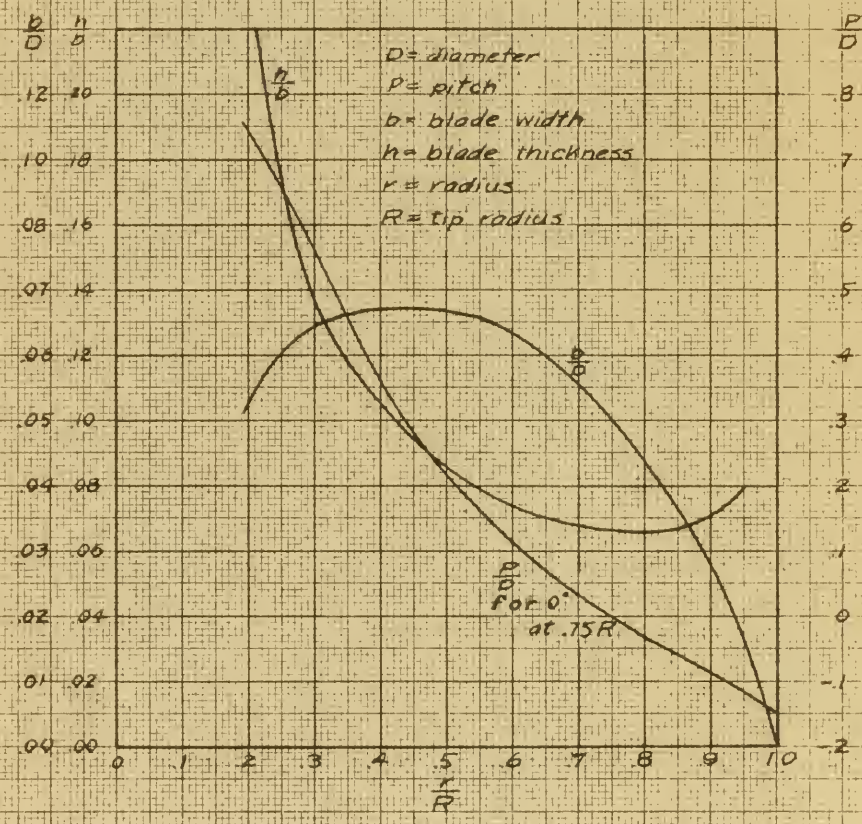

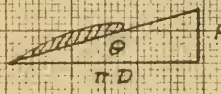

$\frac{P}{D} = \pi \tan \theta$

$\theta = 0°$ at .75 R

FIGURE 10.

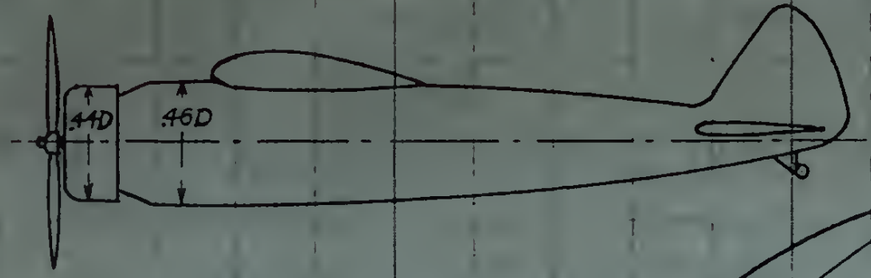

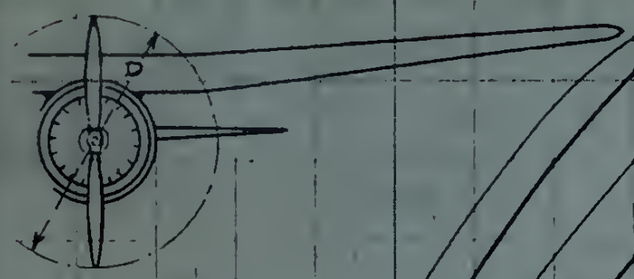

η

90
.80
.70
.60
.50
.40
.30
.20
.10
.00

36°
32°
28°
24°
20°
16°

β=12° at .75 Radius

36°
32°
28°
24°
20°
16°

β=12° at .75 Radius

1.5
1.0
.5

$\frac{V}{nD}$

Line of max. η for C_S

0 .5 1.0 1.5 2.0 2.5 3.0

$C_S = \frac{\rho^{\frac{1}{5}} V}{n^{\frac{2}{5}} D^{\frac{2}{5}}}$

TWO BLADED PROPELLER CHARACTERISTICS

EFFICIENCY & ADVANCE RATIO VS. SPEED-POWER COEFFICIENT FOR VARIOUS BLADE ANGLES

FROM $\frac{1}{6}$ SCALE MODEL TESTS

CALIF. INST. TECH.
MAY 1935

LT. J.S. RUSSELL USN
LT. H.M. McCOY AC USA

FIGURE 11

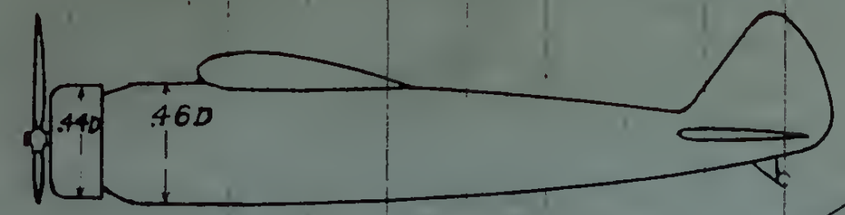

η

.90
.80
.70
.60
.50
.40
.30
.20
.10
.00

$\beta = 32°$ at .75 Radius
28°
24°
20°
16°
12°

$\beta = 32°$ at .75 Radius
28°
24°
20°
16°
12°

1.5
1.0
.5

$\frac{V}{nD}$

Line of max. η for C_s

0 .5 1.0 1.5 2.0 2.5 3.0

THREE BLADED PROPELLER CHARACTERISTICS

EFFICIENCY & ADVANCE RATIO VS SPEED-POWER COEFFICIENT FOR VARIOUS BLADE ANGLES

FROM $\frac{1}{6}$ SCALE MODEL TESTS

CALIF. INST. TECH.
MAY 1935

LT. J.S. RUSSELL USN
LT. H.M. McCOY AC USA

FIGURE 12. $C_s = \frac{\rho^{\frac{1}{5}} V}{n^{\frac{2}{5}} p^{\frac{4}{5}}}$

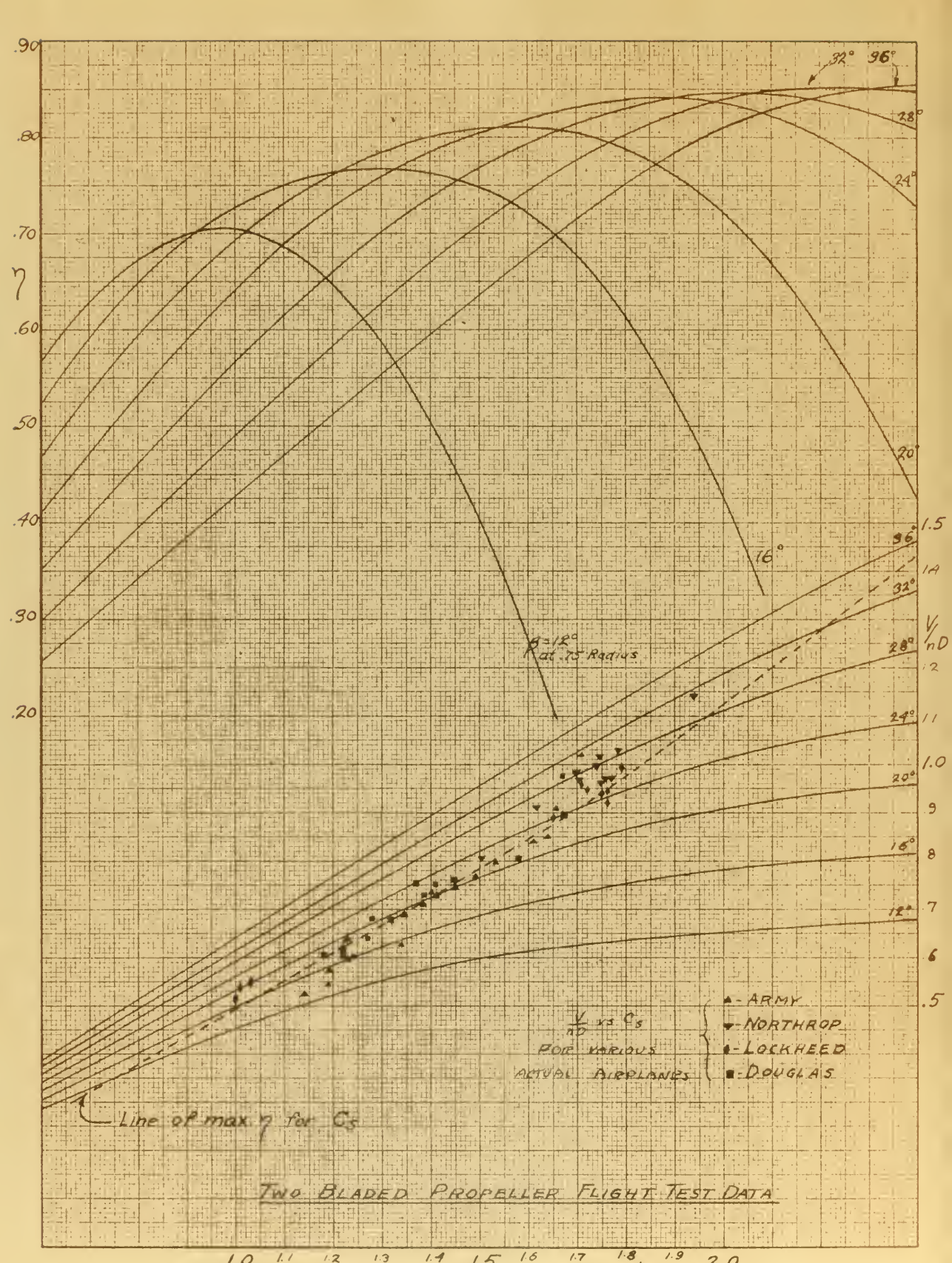

TWO BLADED PROPELLER FLIGHT TEST DATA

FIGURE 13. $C_S = \frac{\rho^{\frac{1}{5}} V}{n^{\frac{2}{5}} P^{\frac{1}{5}}}$

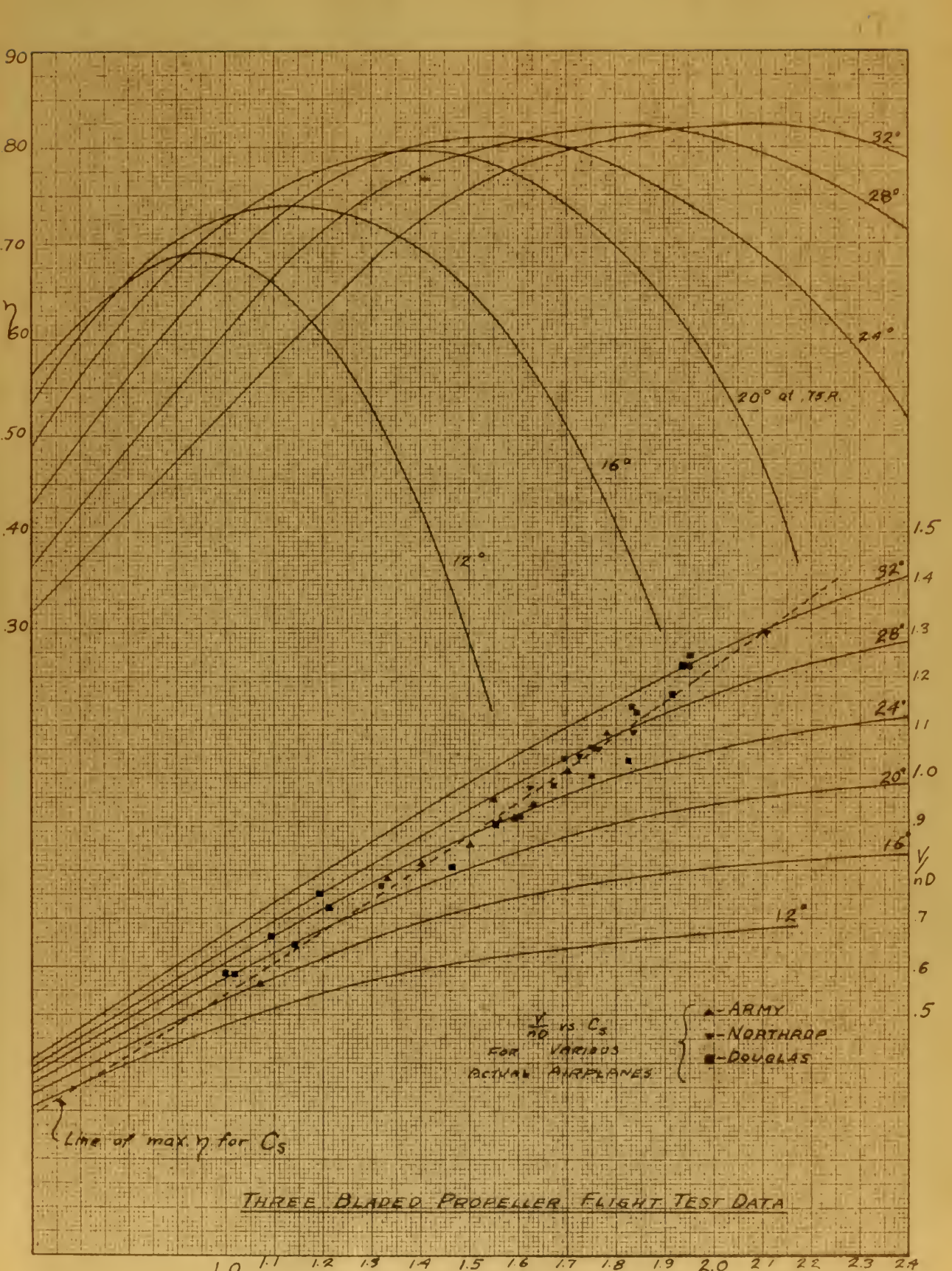

THREE BLADED PROPELLER FLIGHT TEST DATA

FIGURE 14.

DATA ON PROPELLER CHARACTERISTICS

C.L. Johnson
4-24-35

LOCKHEED FLIGHT TESTS

TABLE I

Ship No.	Prop.	Type	Dia.	Design Condition	(True MPH)	B.H.P. Output	R.P.M.	B at 42" (Setting)	V/ND	C	Density Altitude	Accuracy of Test
#1001 Electra	6095-15	2 blade H.S.	8'3"	High Speed at 5000' (Load 7600#)	203	373/eng.	2170	22	.998	1.79	6500'	Fair
#1010 Electra	6095-6	2 blade H.S.	9'0"	High Speed at 5000' (Full load)	203.7	400	2200 (Tip loss)	20	.918	1.76	5000'	Good
#215 Altair	6095-6		9'0"	High Speed at 5000'	215.0	550	2230 (Tip loss)	22	.943	1.75	5000'	Very good
"	"		"	Sea level Cruising	183.5	429	2000	22	.898	1.65	0	Good
#1004 10C Elect.	"		"	High Speed at 6000'	202	450	2080	23	.953	1.72	6000'	Good
"1012 10A Elect.	"		"	Cruising at 10,000'	195	300	2020	22	.945	1.76	9500'	Very good
"1009 10C Elect.	"		"	Cruising at 12,000'	182	281	1850	25	.961	1.71	12,000'	Fair
Above are all high pitch settings - Below are low pitch settings												
#1010	6095-6		9'0"	Single Engine	115	370	2180	14	.517	1.00	7100'	Good
#1004	6095-6		9'0"	"	120	410	2100	17	.557	1.03	6800	Good
#215	6095-6		9'0"	Climb	123	527	2200	16	.547	1.01	3700'	Fair

DATA ON PROPELLER CHARACTERISTICS: NORTHROP FLIGHT TESTS

NORTHROP MODEL	h	T	σ	P	N PROP	V	No BLADES	GEAR RATIO	DIA	β @ .75R		C_s	$\frac{V}{nD}$
W-B	S L	?	1 000	335	2090	206	2	1 1	758	28°7		1 940	1.145
G	7400	"	800	510	2181	215	2	1 1	9.0	21°8		1.750	.965
RT-1	5100	"	85?	735	1920	"	3		9.5	25°0		1.725	1.037
"	5200	"	857	738	1905	217	"	"	"	"		1.750	1.056
"	13000	"	671	426	1750	183	"		"	24.°5		1625	.970
B-G	7800	"	851	428	2040	203	2	"	9	23°0		1.770	974
"	"	"	"	438	2060	204	"	"	"	"		1 760	.968
1-B-1	S.L	"	1000	630	1915	200	"	"	9.5	24°5		1 705	"
2A	6000	"	.836	730	1640	247	3	"	10.25	30°0		2.110	1.293
A	S.L	"	1.000	420	2000	165	2	"	9.0	19°.5		1505	.807
1D	8000	37°	.775	675	1950	221.5	3	"	9 5	24°25		1.765	1.053
"	7000	34°	.811	671	1880	220	2	"	10.0	25.°25		1.785	1.030
1D-5	4000	?	.888	719	1930	215.5	"	"	9.83	"		1.740	1.000
1D-2	8500	48°	.743	714	1950	217.5	3	"	9.5	24.°0		1.695	1.033
"	7400	75°	.738	703	"	219	2	"	10.0	24°25		1 700	.983
2D	8000	59°	.742	689	1960	223	"	"	9 83	25°.75		1.745	1.020
1D-3	3200	86°	.848	633	2040	201	"	"	9 5	22°0		1620	.913

TABLE 2.

Analysis PROPELLERS
Prepared by R007
Date 5-16-35
Copied 5/14/15 H.M.C.

DOUGLAS AIRCRAFT COMPANY, INC.

PLANE	ENGINE	PROP. DIA	BLADE B	SETTING @ 42" (b) .15R	$h_{CRIT.}$	V_{CRIT}	POWER P	R.P.M. N	GEAR RATIO	R.P.M. PROP	$\sigma^{1/5}$	P 7 FACTOR	P' 66 FACTOR	C_S	$\frac{V}{nD}$
O-43A	[illegible] V 1570-34	9'10"	3	24 1/4° a	S.L.	190.8	675	2450	7:5	1750	1	472.5	450	1.67	.976
C-29	P&W R 1340-23	9'0"	2	16 1/2 a	"	154 6	2x575	2220	1:1	2220	1			1.28	631
O 38E	P&W R 1640 4	8'9"	3	18 6 a	"	153.8	625	2000	1:1	2000	1	437.5	417	1.32	773
YO 31C	CURTISS V 1570C	9'10"	3	24.2 a	"	195	600	2450	7:5	1750	1	420	400	1.75	.997
YIC-26A	? P&W YIR 985 B	9'	2	15.2 a	"	137.3	2x350	2095	1:1	2095	1			1.27	.641
XO-35	CURTISS V 1570C	9'10"	3	23.2 a	"	178.3	2x600	2465	7 5	1760	1	420	400	1 60	.907
XB-7	[illegible]	8'5 1/4"	2	19 a	"	174.2	2x600	2410	1:1	2410	1			132	.754
O 25C	CURTISS V 1570	10'9"	2	21.6 a	"	161	600	2460	7:5	1756	1			1.45	.750
BT 2B	P&W R 1340 A	9'3"	2	143 a	"	133.5	450	2100	1:1	2100	1			1.18	.605
O-32	P&W R 1340 B	10'	2	16.8 a	"	133	450	1920	1:1	1920	1			1.22	.610
XO 39	CURTISS V 1570	10'9"	2	22 a	"	156.5	600	2385	7:5	1703	1			1.41	.752
O 32A	P&W R [illegible]	9'10"	2	15.3 a	"	129.8	410	1985	1:1	1935	1			122	.600
O 22	P&W SR 1340C	10' 1/2"	2	15.5 a	5000	142.3	450	2095	1:1	2095	.977			1.23	.596
O-25	CURTISS V 1570	10'9 1/2"	2	22 a	S.L.	156.6	600	2450	7:5	1750	1			1.39	.730
XO-14	WRIGHT R 1902	8'10"	2	14.1 a	"	121.4	236	2020	1:1	2020	1			1.24	.599
OC1A (S.E)	SDG F-2	11 1/2	3	23 3/4	6500	111	700	2160	3:2	1440	.962	490	466	1.00	.590
DC 1		11.5'	3	24 b	8100	211.2	710	1920	16:11	1320	.952	497	473	1.95	1225
DC 2 KLM # 1	F-2	11'	3	25 b	4100	202	720	1840	16:11	1300	.976	504	480	1.95	1.245
DC 2 STD OIL	SDG	11.5'	3	21 1/2 b	6500	212	700	2150	3:2	1434	.962	490	467	1.84	1.129
DC 2 AM. AIR	F 1	11 5'	3	25 b	8100	197.8	710	1935	16:11	1330	.952	497	473	1.83	1.138
?	SIA2-6	11.5	3	20 1/2 b	7000	214.5	800	2400	3:2	1600	.959	560	533	1.82	1.027
VAND. DOLPH	GB	9'	2	15 b	5000	145 5	400	2090	1:1	2090	.971			1.32	.681
?	YR(1820-25	12.5	3	19 1/2 b	2800	163.5	750	1950	16:11	1340	.984	525	500	1.55	.895
?	?	11.5	3	23.8 b	S.L.	167.5	825	2400	3:2	1600	1	578	550	1.46	.802
XFD-1	S2K 1535	10'	2	24.75 b	8900	208.2	700	2500	4:3	1875	.948			1.67	.978
PAN AM GRACE DC	F-3	11'	3	25° LP	8000	131	675	2030	16:11	1395	.954	473	450	1.19	.752
"	"	"	3	34 1/2 HP	"	208	700	1930	16:11	1327	.954	490	466	1.93	1.255
STD. OIL DC.	SDG	11 1/2'	3	21 LP	7000	116	522	2050	3:2	1367	.959	365	348	1.14	.649
"	"	11 1/2'	3	30.5 HP	"	203	650	2010	"	1340	"	455	433	191	1.16
DC-2 KLM (S.E)	F-2	11'	3	25°	4100	117	694	2060	16:11	1416	.977	486	462	1.08	.661
STD. OIL DC	E Horn.	11 1/2'	3	21	7000	110	651	2150	3:2	1433	.959	456	433	1.02	.587
AM AIR DC	F-3	11 1/2	3	24.5	7000	129	680	1980	16:11	1362	.959	476	453	1.21	725

TABLE 3

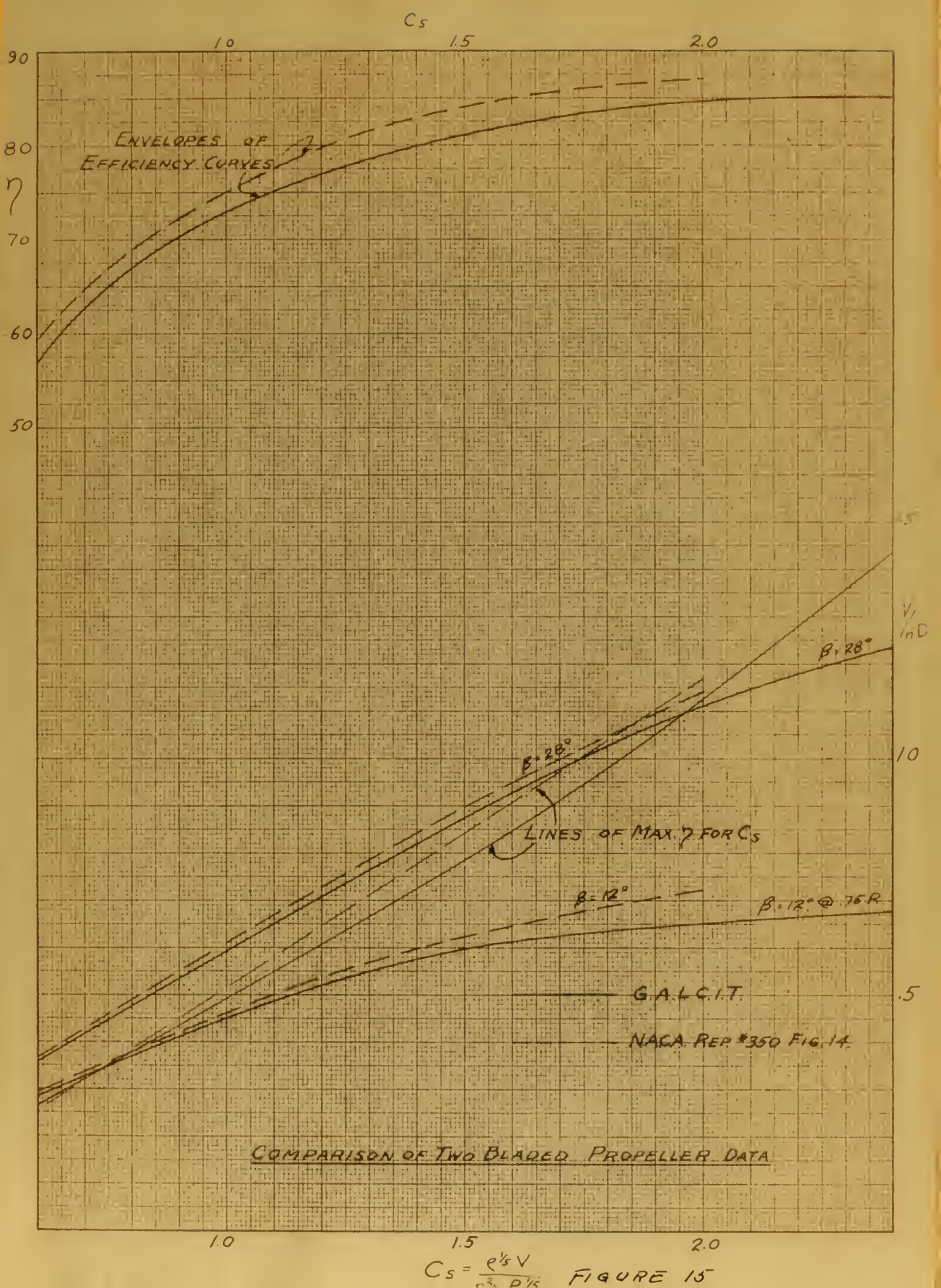

COMPARISON OF TWO BLADED PROPELLER DATA

FIGURE 15

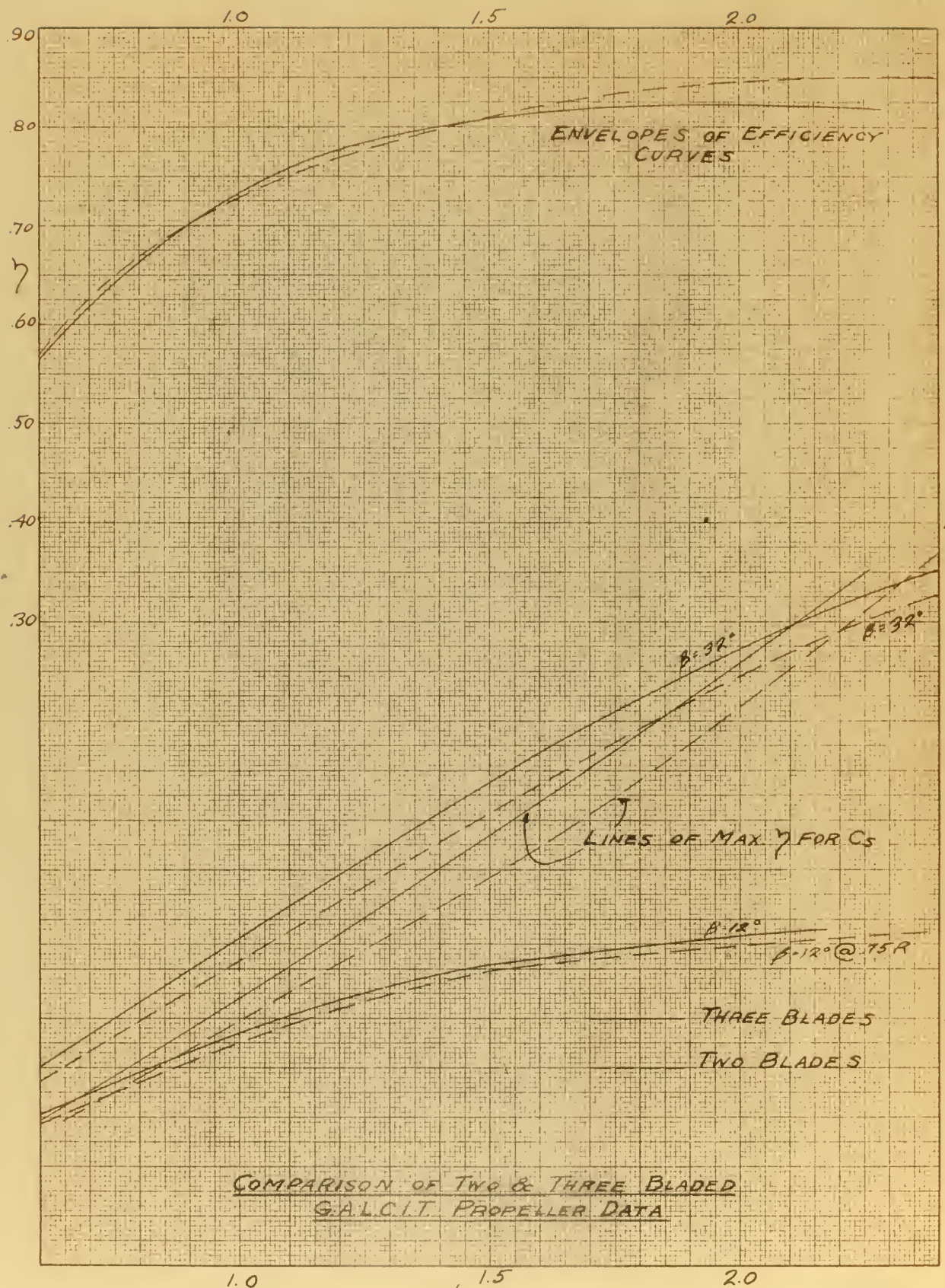

COMPARISON OF TWO & THREE BLADED G.A.L.C.I.T. PROPELLER DATA

$C_S = \frac{\rho^{1/5} V}{n^{2/5} P^{1/5}}$ FIGURE 16.

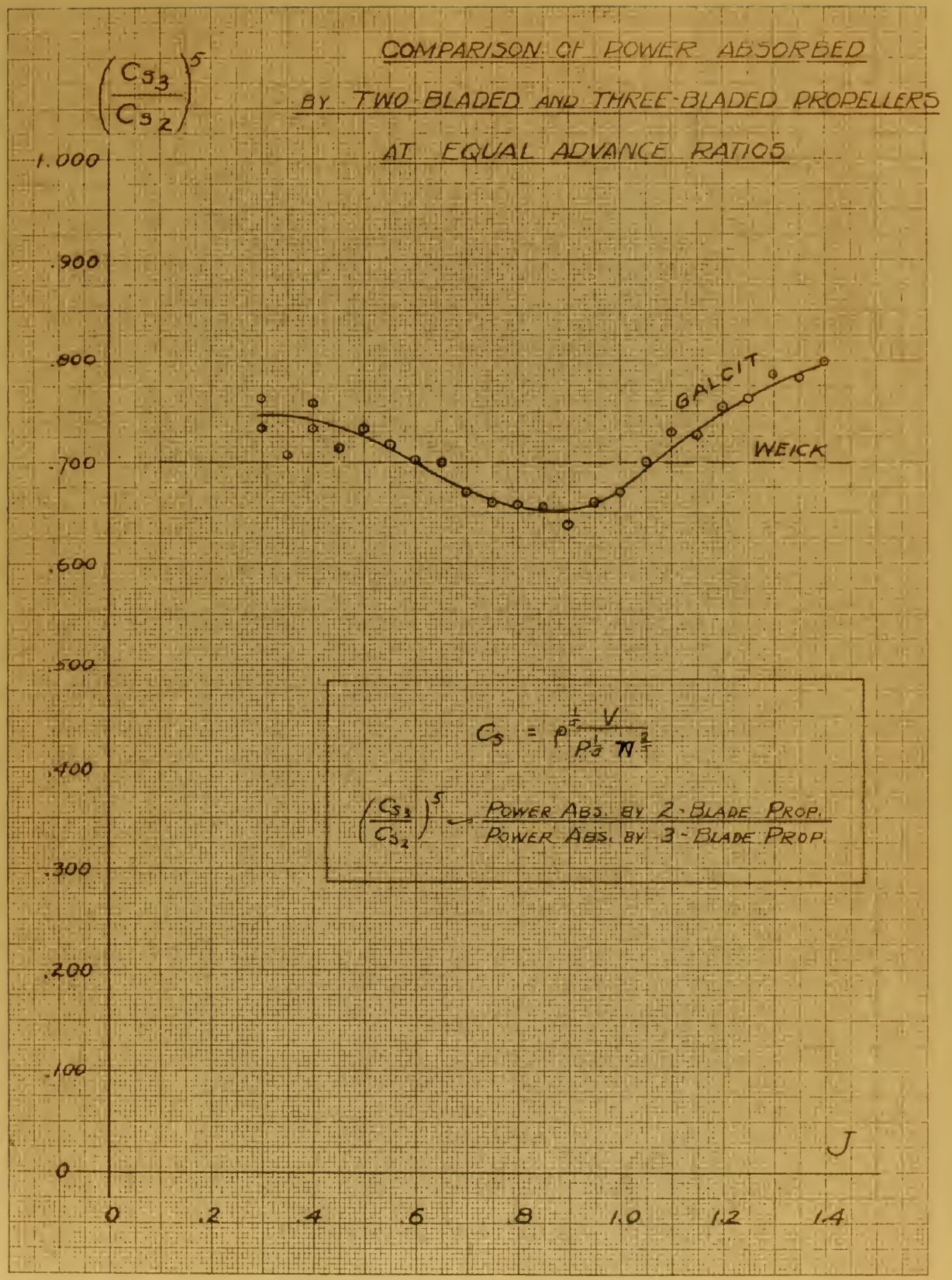
COMPARISON OF POWER ABSORBED
BY TWO-BLADED AND THREE-BLADED PROPELLERS
AT EQUAL ADVANCE RATIOS
$\left(\frac{C_{S_3}}{C_{S_2}}\right)^5$
1.000
.900
.800
.700
.600
.500
.400
.300
.200
.100
0
0
.2
.4
.6
.8
1.0
1.2
1.4
J
GALCIT
WEICK
$C_S = \rho^{\frac{1}{5}} \frac{V}{P_3^{\frac{1}{5}} n^{\frac{2}{5}}}$
$\left(\frac{C_{S_3}}{C_{S_2}}\right)^5 = \frac{\text{POWER ABS. BY 2-BLADE PROP.}}{\text{POWER ABS. BY 3-BLADE PROP.}}$

FIGURE 17

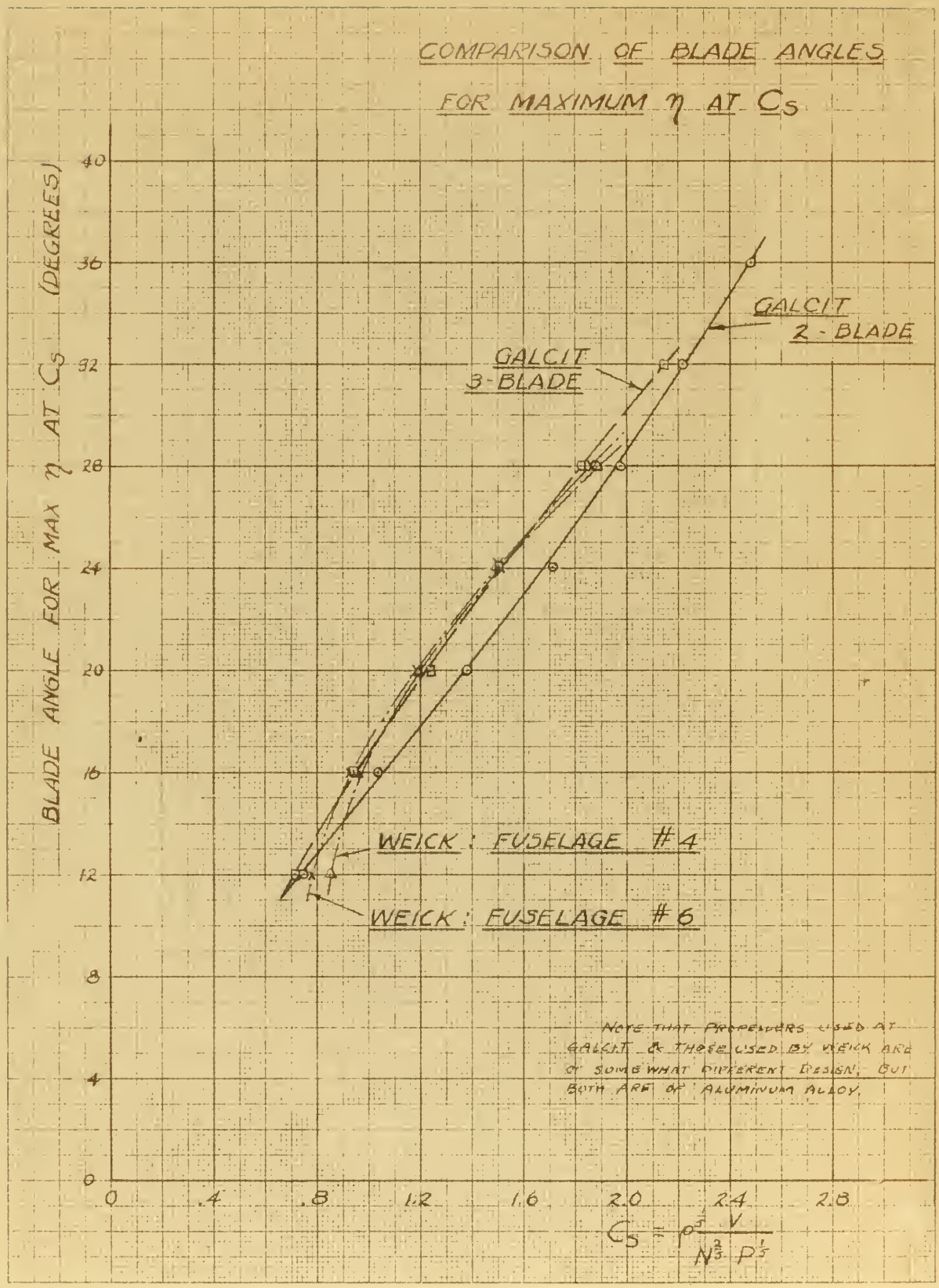
COMPARISON OF BLADE ANGLES
FOR MAXIMUM η AT C_s
BLADE ANGLE FOR MAX η AT C_s (DEGREES)
40
36
32
28
24
20
16
12
8
4
0
0
.4
.8
1.2
1.6
2.0
2.4
2.8
$C_s = \rho^{\frac{1}{2}} \frac{V}{N^{\frac{2}{5}} P^{\frac{1}{5}}}$
GALCIT 2-BLADE
GALCIT 3-BLADE
WEICK : FUSELAGE #4
WEICK : FUSELAGE #6
NOTE THAT PROPELLERS USED AT GALCIT & THOSE USED BY WEICK ARE OF SOMEWHAT DIFFERENT DESIGN, BUT BOTH ARE OF ALUMINUM ALLOY.

FIGURE 18.

PART TWO

Airplane Characteristics Power-On

Power introduces another dimension into wind tunnel calculations in that it is necessary to specify under what power condition the model is acting. However, of the infinite amounts of power input which might be investigated for every attitude of the airplane, only certain ranges are of practical importance. In order to obtain an estimate of the range of powers which it was felt desirable to investigate, a typical conventional airplane corresponding to the model was considered. The upper limit on power was taken as that corresponding to the maximum power available for such a plane as a function of its velocity at sea-level. The lower limit was taken as that corresponding to the power required for level flight at sea-level as a function of velocity. In order that the results might be applicable to other normal planes with somewhat different characteristics, the range of powers investigated was considerably extended beyond these two limits. It should be explicitly pointed out that the characteristics assumed for the full size airplane are used only to determine the limits of power investigated and do not enter into the determination of the effects of power. In order to present the stability and pitching moment results, it was also necessary to assume a center of gravity location relative to the mean aerodynamic chord. This was chosen from the full scale characteristics of the typical conventional airplane mentioned above.

The typical airplane was taken as the Lockheed Vega since its geometrical form, wing section, etc. correspond fairly closely to those of the model. The following full scale data were assumed: Weight, W = 5000 lbs.; center of gravity at 36% of the mean aerodynamic chord and four inches above the thrust line, and maximum brake horsepower 550.

From model tests were taken:

Equivalent parasite area, p: 6.44 ft.^{2}

Airplane efficiency factor, e: .89

Maximum propulsive efficiency, η_{max}: .825

Blade angle at .75 radius, β: 30.3°

Revolutions per minute at maximum power, N: 1350

These data in combination with the physical dimensions of the model to full scale gave, in Oswald's notation: (see NACA Report 408)
$l_s = 3.23$, $l_p = 777$, $l_t = 11$, $\Lambda = 8.5$.

A table of thrust horsepower required against velocity was then made up using sinking speed due to parasite loading w_{s_p}, and sinking speed due to effective span loading w_{s_s}, at various velocities.

Thrust horsepower available at velocity was determined approximately by $R_J = \frac{R_V}{R_T}$; $-R_J$ and β to get C_S; $-C_S$, η, to get Thp_a.

The standard thrust horsepower available and thrust horsepower against V curves were transmuted to a form suitable for wind tunnel work. The ordinate, power, via η, V, and C_S, became J; and the abscissa V via l_w and C_L became α_u. (α_u = wind tunnel angle of

attack).

The conventional thrust horsepower available and required curves are shown in figure 19. These two curves converted to a form suitable for wind tunnel work are represented in figure 20.

The appropriate wind tunnel "q" was determined by examining data of T_c against J from previous wind tunnel runs.

A vertical traverse was made across the power curves using "n" as the controlled variable, as indicated in figure 20. For example, at a wind tunnel angle of attack of $+2^\circ$ a wind tunnel velocity corresponding to $q = \frac{\rho V^2}{2} = 10$ grams per square centimeter, was used, and the revolutions per second of the model propeller were varied in seven equal increments from 69 to 112 r.p.s. It is evident then that all power conditions, from that somewhat under the power required for level flight, to that corresponding to somewhat more than maximum power output, were covered. This was the laboratory procedure for the power-on condition.

The effects of power on lift, drag, and pitching moment were desired, in order to furnish information on free flight performance, stability, and control characteristics of high wing monoplanes.

Effect of Power on Lift, Drag, and Performance

In order to give a satisfactory discussion of this subject, it is necessary to analyze the problem somewhat more closely than is customary. With this in view, let us consider an airplane in

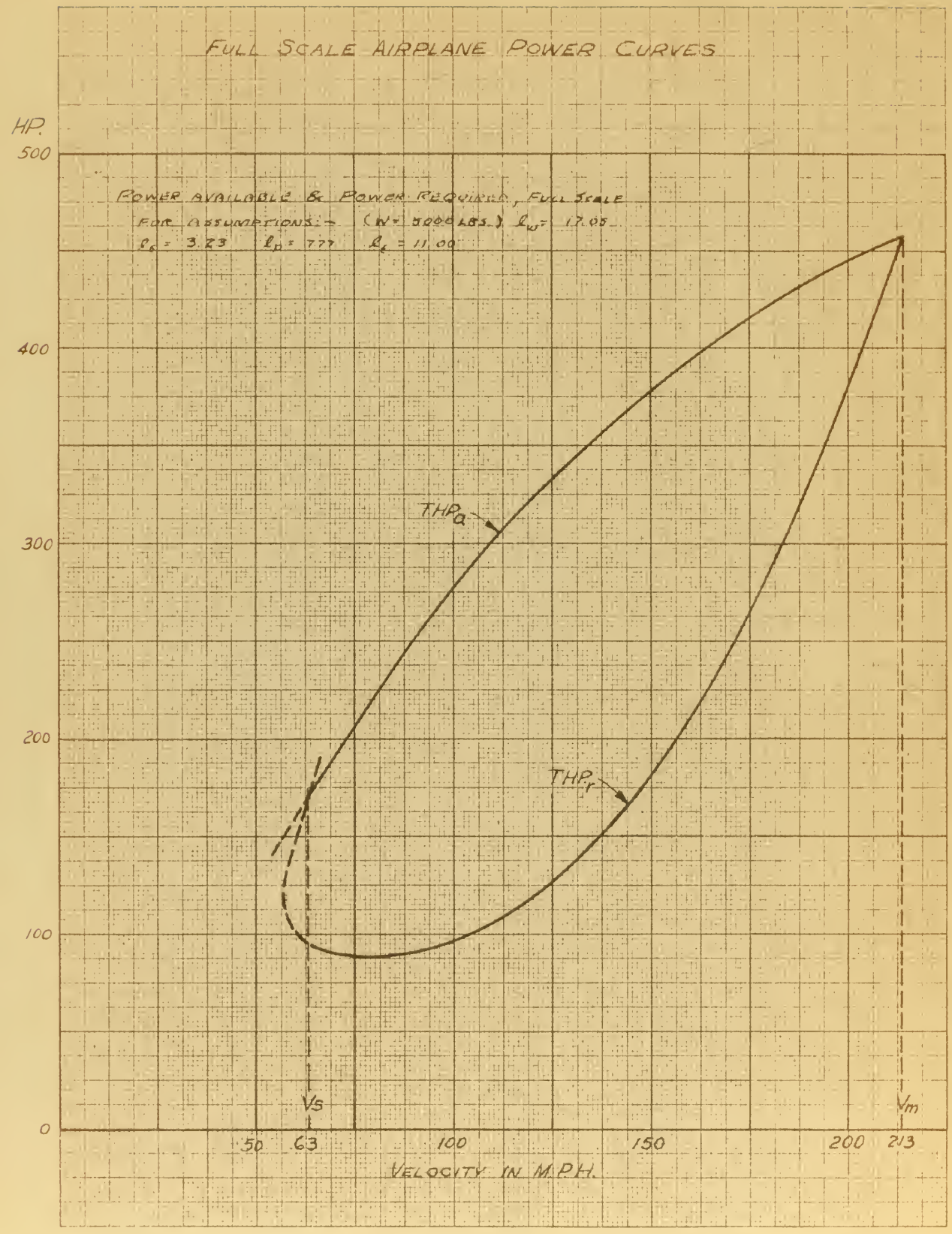
FULL SCALE AIRPLANE POWER CURVES
HP.
500
400
300
200
100
0
POWER AVAILABLE & POWER REQUIRED, FULL SCALE
FOR ASSUMPTIONS:- (W = 3000 LBS.) ℓ_w = 17.05
ℓ_c = 3.23 ℓ_p = 777 ℓ_f = 11.00
THP_a
THP_r
Vs
Vm
50
63
100
150
200
213
VELOCITY IN M.P.H.

FIGURE 19

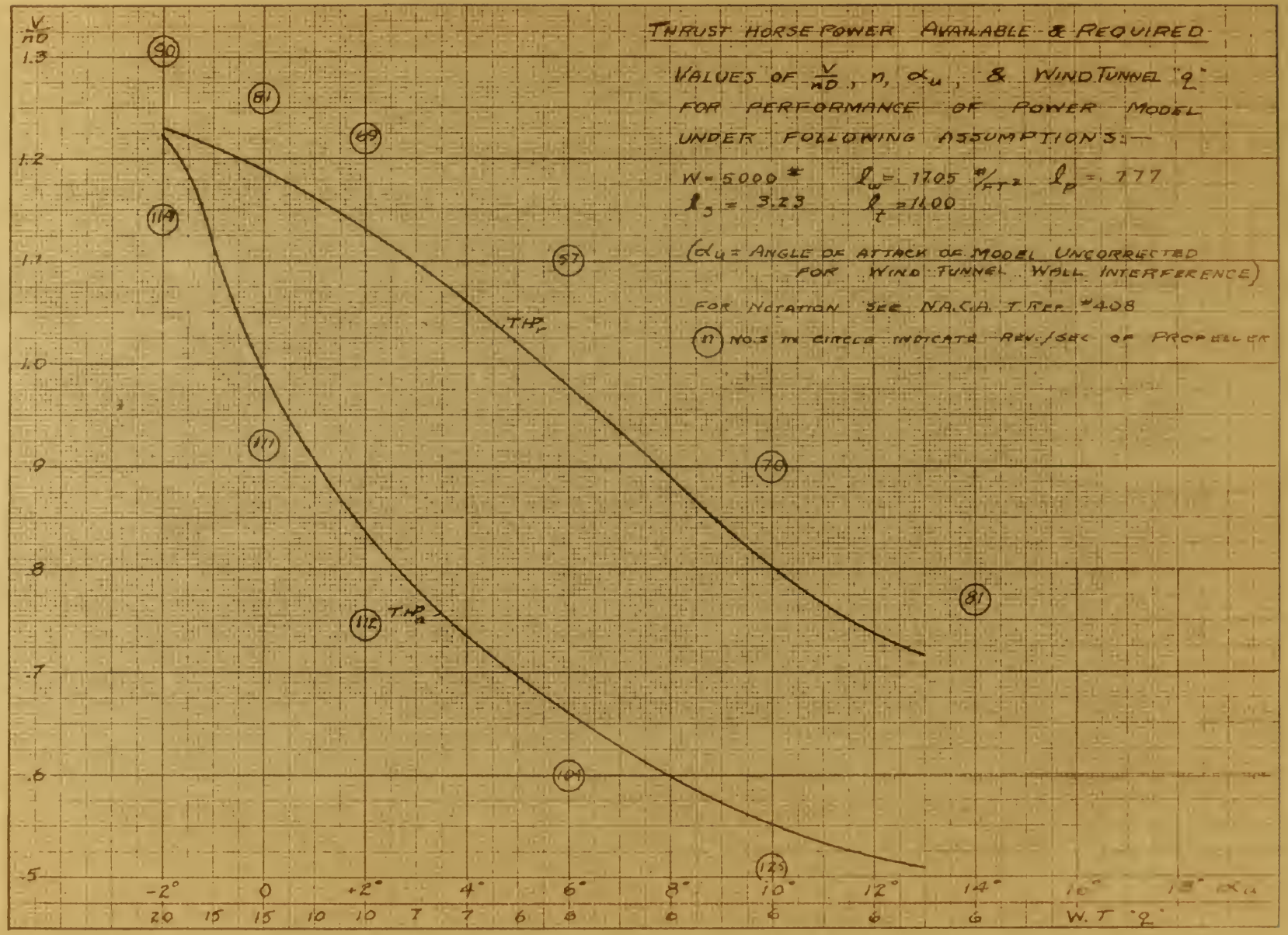
THRUST HORSE POWER AVAILABLE & REQUIRED
VALUES OF V/nD, n, α_u, & WIND TUNNEL "q" FOR PERFORMANCE OF POWER MODEL UNDER FOLLOWING ASSUMPTIONS:—
W = 5000 #
ρ_w = .1705 #/FT²
ρ_p = .777
l_s = 3.23
l_t = 1.400
(α_u = ANGLE OF ATTACK OF MODEL UNCORRECTED FOR WIND TUNNEL WALL INTERFERENCE)
FOR NOTATION SEE N.A.C.A. T. REP. #408
(11) NO.S IN CIRCLE INDICATE REV./SEC OF PROPELLER
THP_r
THP_a
V/nD
1.3
1.2
1.1
1.0
.9
.8
.7
.6
.5
-2°
0
+2°
4°
6°
8°
10°
12°
14°
16°
18°
α_u
20 15 15 10 10 7 7 6 6 6 6 6 6
W.T "q"

FIGURE 20

climbing (or gliding) unaccelerated flight. The forces acting in the direction of the flight path may be split up into a thrust, a drag, and a gravity force as shown in the accompanying diagram.

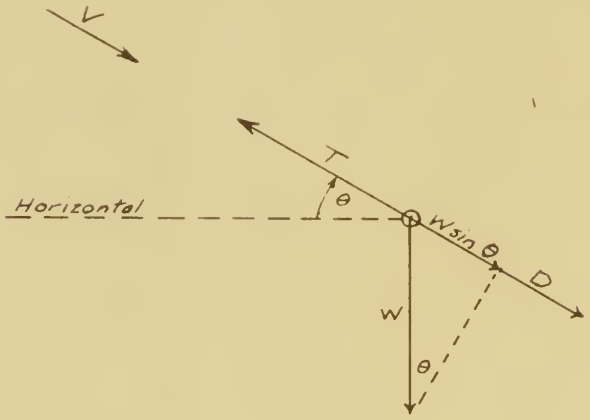

where

T = component of thrust in the direction of the flight path,

D = drag,

θ = angle of climb,

W = weight,

V = velocity along the flight path.

The equilibrium condition is

1) $$D + W \sin \theta = T$$

The precise definition of D and T has not yet been given. However, before discussing this question, let us first transform 1) to a more familiar and convenient form. Multiplying by V, expressing T in terms of brake horsepower P, and a propeller efficiency η,

and introducing the drag coefficient, C_D, we obtain:

2) $$C_D(\alpha,J)\, q\, S\, v + W \sin\Theta \cdot V = P\, \eta'(\alpha,J)$$

where the variables upon which C_D and η' may depend have been explicitly indicated. It will be noted that equation 2) is just the usual performance equation.

We have just stated that the precise significance of D and T in 1) had not yet been given. This means that in 2), C_D and η' have not yet been exactly defined. Actually we may define either one in a rather arbitrary fashion, the other is then determined by the fact that the forces must be in equilibrium, i.e. equation 2) must be satisfied.

It has been customary in the past to define $C_D(\alpha,J)$ by equating it to $C_{D_o}(\alpha)$ which is the drag coefficient of the airplane without propeller. Then in order that 2) may be satisfied, the propeller efficiency $\eta'(\alpha,J)$ should be replaced by a propulsive efficiency $\eta(\alpha,J)$ determined from wind tunnel tests on an airplane or model with propeller running, and for all pertinent values of J and α. 2) would then take the form

3) $$C_{D_o}(\alpha)\, q\, S\, V + W \sin\Theta \cdot V = P\, \eta(\alpha,J)$$

Practically all propulsive efficiency investigations in the past have been restricted to the case of zero inclination of the thrust axis, so that the dependence of η on J is well known, while its dependence on α has been very little discussed. It was one of the essential aims of the present series of tests to furnish data on

this variation of propulsive efficiency with thrust axis inclination. The data so obtained could be presented in the form of a series of normal propulsive efficiency charts each corresponding to a definite value of α or thrust axis inclination. However, the complications introduced into normal performance calculations, through the necessity of using such a family of propulsive efficiency charts, would be so overwhelming that it is very doubtful whether the data would be of any practical service. An entirely different method of presenting the results, based on a rather different point of view with respect to the performance equation has been suggested by Dr. Clark B. Millikan, and gives the data in such a form that the designer can use them in performance estimation without any essential modification to the normal calculation procedure.

In introducing this new method we return to equation 2) and replace $\eta'(\alpha,J)$ by a propulsive efficiency $\eta_o(J)$ which is determined from measurements at zero inclination of the thrust axis, i.e. η_o is just the propulsive efficiency which is customarily given in the standard propeller charts. Then in order that 2) may be satisfied, we must replace C_D by an effective drag coefficient C_{D_e}, so that the performance equation now takes the form:

4) $$C_{D_e}(\alpha,J)\, q\, S \cdot V + W \sin\theta \cdot V = P\, \eta_o(J)$$

(Note that at zero inclination of the thrust axis, equations 3) and 4) are identical, i.e. $\eta = \eta_o$ and $C_{D_e} = C_{D_o}$). With this equation, performance is calculated in exactly the normal manner, using the standard propulsive efficiency charts, the only

modification being that C_{D_e} is used instead of C_{D_o}. We shall return later to the discussion of how this modification is accomplished and shall see that no considerable additional labor is required. We must first, however, investigate the manner in which C_{D_e} may be determined from our wind tunnel tests.

In the accompanying diagram, the forces in the direction of the relative wind which act on the model mounted in the wind tunnel are indicated. R is the resultant force exerted by the model on the drag rigging, taken as positive in the direction of the drag force. Hence the external force which the drag rigging exerts on the model is R, taken as positive in the direction of the thrust. The diagram, which has been drawn with all forces positive, is exactly analogous to the previous free-flight diagram except that the wind-tunnel diagram corresponds to a case in which $T < D$, i.e. to an airplane in gliding rather than climbing flight. The condition that the forces be in equilibrium leads to the equation

$$D = T + R,$$

or multiplying by V and defining the drag coefficient and propulsive efficiency exactly as in 4):

5) $$C_{D_e}(\alpha, J)\, q\, S\, V - R\, V = P\, \eta_o(J)$$

Comparing with 4), we see that the wind tunnel and free-flight equations are identical if

6) $$R = -T \sin \theta$$

This means that the resultant force exerted by the drag balance on the model plays exactly the same role in the wind tunnel as does the component of the gravity force along the flight path in unaccelerated free flight. If we determine values of C_{D_e} in the wind tunnel for a series of values of α, the former are identical with the values of C_{D_e} in free flight for the corresponding values of $W \sin \theta$.

It appears now that we must determine C_{D_e} as a function of three independent parameters α, J, and P. However, it is easy to see that only two are independent. Dividing 5) by $q S V$ and introducing the coefficient of resultant force $C_R = R/qS$ we obtain

$$C_{D_e}(\alpha, J) = C_R + \frac{P \eta_o}{q S V}$$

But, at a given α, C_R is a function only of J, i.e. $J = J(\alpha, C_R)$. Hence, introducing torque and revolutions per second,

$$C_{D_e}(\alpha, C_R) = C_R + \frac{2\pi Q}{q S} \frac{n}{V} \eta_o$$

It is convenient to replace the variable α by the lift coefficient C_L since the latter is the essential parameter in the free flight case. If we define the lift as the resultant aerodynamic force perpendicular to V (including any contribution from inclined thrust) then the wind tunnel measurements give $\alpha = \alpha(C_L)$, (cf. Fig. 22). Hence we obtain the final equation for the determination of C_{D_o}:

7) $$C_{D_e}(C_L, C_R) = C_R + \frac{2 \pi Q}{\text{Dia.} \cdot q S} \frac{\eta_o(J)}{J}$$

C_L, C_p, [illegible], [illegible], and J are measured in the wind tunnel, D is, and S are known, and $\eta_o(J)$ is obtained from propulsive efficiency charts corresponding to zero thrust inclination.

It now only remains to express C_R in terms of a parameter having a significance in free flight. If we follow the definition given above and take L as the resultant aerodynamic force perpendicular to the relative wind (flight path) then we see from the first diagram of this section that for unaccelerated, rectilinear flight

$$L = W \cos \theta.$$

Combining with 6)

$$\frac{R}{L} = - \tan \theta,$$

or finally

8) $$C_R = - C_L \tan \theta.$$

Hence our wind tunnel observations finally give

9) $$C_{D_\theta} = C_{D_\theta}(C_L, \theta)$$

The complete results may then be expressed in the form of a family of polars of C_{D_θ} vs. C_L, each polar corresponding to a constant angle of climb (or glide) θ. These polars will have somewhat the character of those in the accompanying sketch, possessing a common intersection at the C_L corresponding to zero thrust axis inclination, which will normally be near the high speed attitude of the airplane.

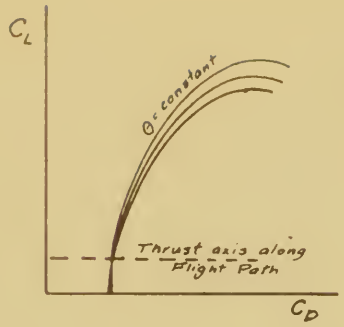

We return finally to the question of how such data can most easily be used in performance analyses. Following Oswald we may define the airplane efficiency factor e by the equation

10) $$C_{D_\theta} = \frac{C_L^2}{e \cdot \pi\, AR} + C_{D_p}$$

(AR = aspect ratio = b^2/S, and C_{D_p} = parasite drag coefficient) where e is chosen so as to determine as nearly a constant value of C_{D_p} as is possible over the flying range. Now since all of the polars will normally intersect close to the axis, $C_L = 0$, C_{D_p} will be practically the same for all, and the effect of variations in θ can be taken into account by varying e only. This means that we may present all of the wind tunnel data pertinent to normal performance calculations by giving

11) $$e = e(\theta).$$

Performance calculations may then be carried out in the conventional manner except that for any particular angle of climb the appropriate value of e, and hence of span loading, must be taken.

Before proceeding to a discussion of the experimental results in the light of the above considerations, it might be pointed out that the angle of climb as introduced above appears to be the most satisfactory dimensionless parameter which can be found for describing the condition of power output under which an airplane is operating. Not only the performance characteristics of this section, but also the

stability and control results of the next are presented in terms of this convenient parameter θ.

The experimental lift and drag results are given in Figs. 21 and 22. Fig. 21 shows that the addition of power has made very little change in the conventional polar curve at low lift coefficient. There is, as we might expect, an extension to higher lift coefficients due to (1) liftwise force generated by the propeller when inclined to the free air stream velocity, and (2) the effect of the increase in velocity of the air stream over the center of the wing in delaying the break down of flow. (This may be considered as due to the scouring action of the accelerated flow on regions of incipient break down of flow as in the interference drag region at the intersection of wing and fuselage). In Fig. 21, power conditions other than that for level flight are omitted for clarity. They coincide, practically identically with the level flight curve given up to the point where the power-on polar departs from the power-off (no propeller) polar. Beyond this point increasing deficiencies in power corresponding to increasingly steeper gliding paths, cause the power-on polar to approach the power-off polar more and more closely.

Fig. 22 shows the effect of power on the lift against angle of attack curve. The velocity curve for the equilibrium condition of flight is superimposed and it is interesting to note that the velocity at stalling, and also for landing at a given attitude, is reduced by about 4 miles per hour in the power-on condition.

The practical results of this portion of the investigation are, then, that for high

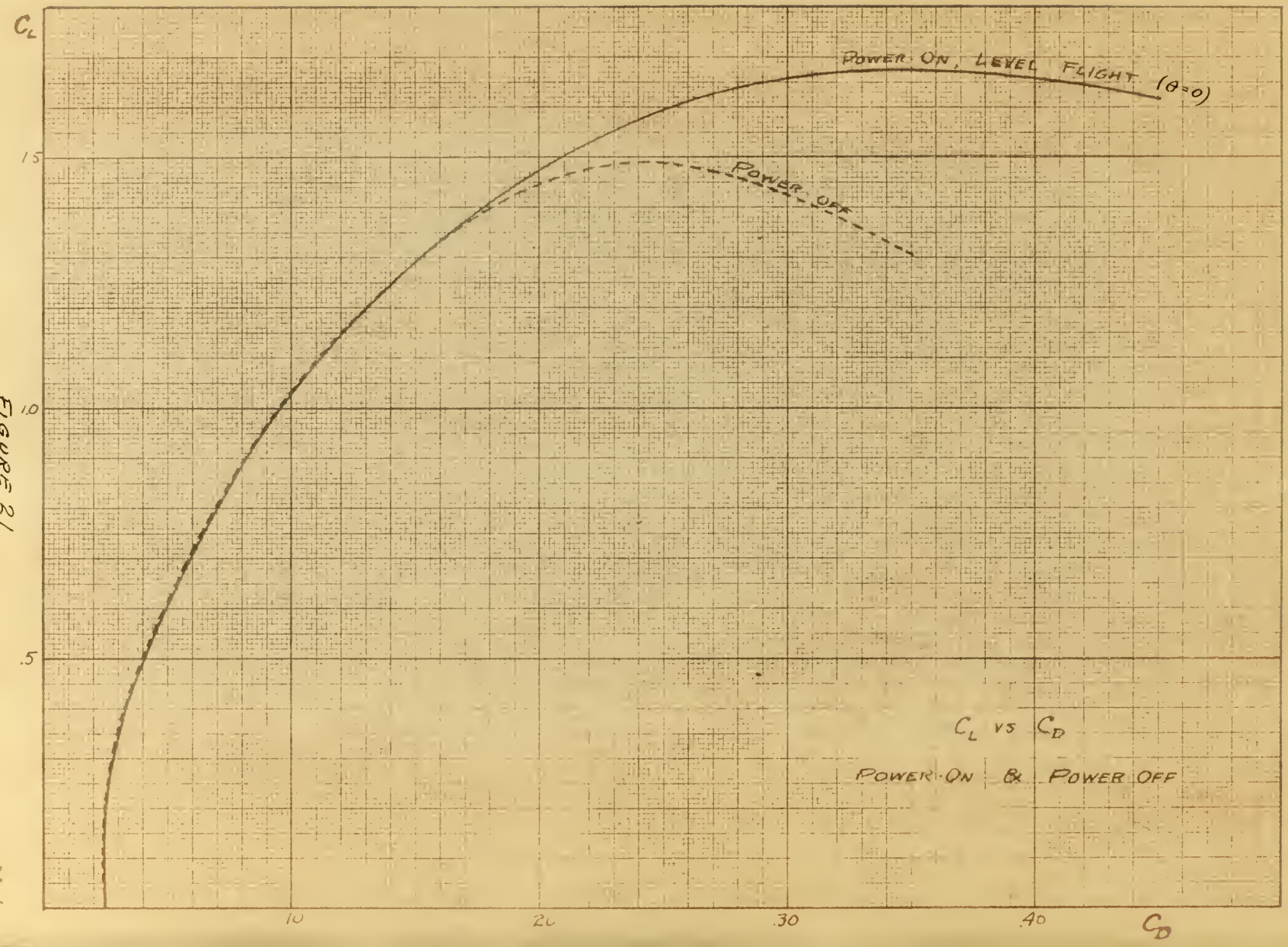

FIGURE 21

10231

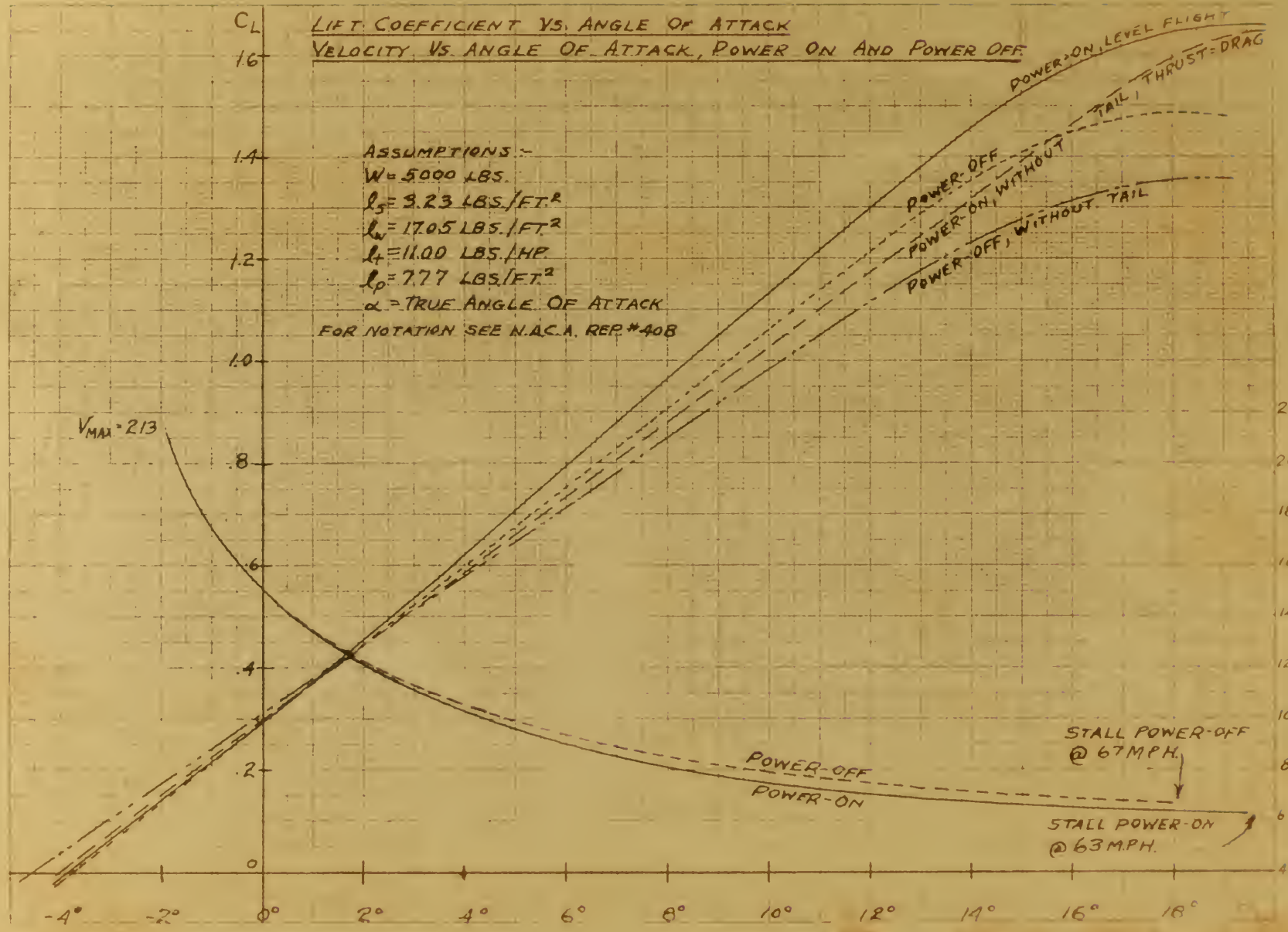
C_L
LIFT COEFFICIENT VS. ANGLE OF ATTACK
VELOCITY VS. ANGLE OF ATTACK, POWER ON AND POWER OFF
ASSUMPTIONS :-
W = 5000 LBS.
l_s = 3.23 LBS./FT.²
l_w = 17.05 LBS./FT.²
l_t = 11.00 LBS./HP.
l_p = 7.77 LBS./FT.²
α = TRUE ANGLE OF ATTACK
FOR NOTATION SEE N.A.C.A. REP. #408
POWER-ON, LEVEL FLIGHT
TAIL THRUST = DRAG
POWER-OFF
POWER-ON, WITHOUT TAIL
POWER-OFF, WITHOUT TAIL
V_{MAX} = 213
POWER-OFF
POWER-ON
STALL POWER-OFF @ 67 M.P.H.
STALL POWER-ON @ 63 M.P.H.
1.6
1.4
1.2
1.0
.8
.6
.4
.2
0
-4°
-2°
0°
2°
4°
6°
8°
10°
12°
14°
16°
18°
220
200
180
160
140
120
100
80
60
40
VELOCITY (M.P.H.) LEVEL FLIGHT

FIGURE 22

wing monoplanes similar to that in the tests, power-on increases $C_{L_{max}}$ quite noticeably, while ϵ, power-on, may be taken as identical with ϵ, power-off, for performance calculations.

Effect of Power on Pitching Moment, Static Longitudinal Stability, and Elevator Effectiveness

Pitching moment coefficients about the assumed c.g. position were determined in the usual manner from the observed pitching moment about the axis of rotation of the model, the lift force, and the resultant drag force R. Fig. 23 shows the effect of power on the pitching moment vs. lift curve. The definite destabilizing effect is apparent. In the case of the wing and fuselage alone, as well as that of the complete model, the slope of the moment curve has been given a positive increment by the addition of power. The effect of varying degrees of power is shown in the curve for the complete model - contours are drawn in for tan θ = $\pm$.05, $\pm$.10, etc., in equal increments. It appears desirable to extend the study to the case of the idling propeller where the power is negative, i.e. a braking power, which would involve developing a negative torque equal to the friction torque of the idling engine (itself a rather variable quantity). Developing and recording a negative torque was quite feasible with our apparatus but involved operating delays which would have drawn out further an already extended investigation.

Fig. 24 shows the effect of power on the effectiveness of the elevator. It is seen that the effectiveness of this control at all "up" angles, and at the larger "down" angles, is enhanced by the

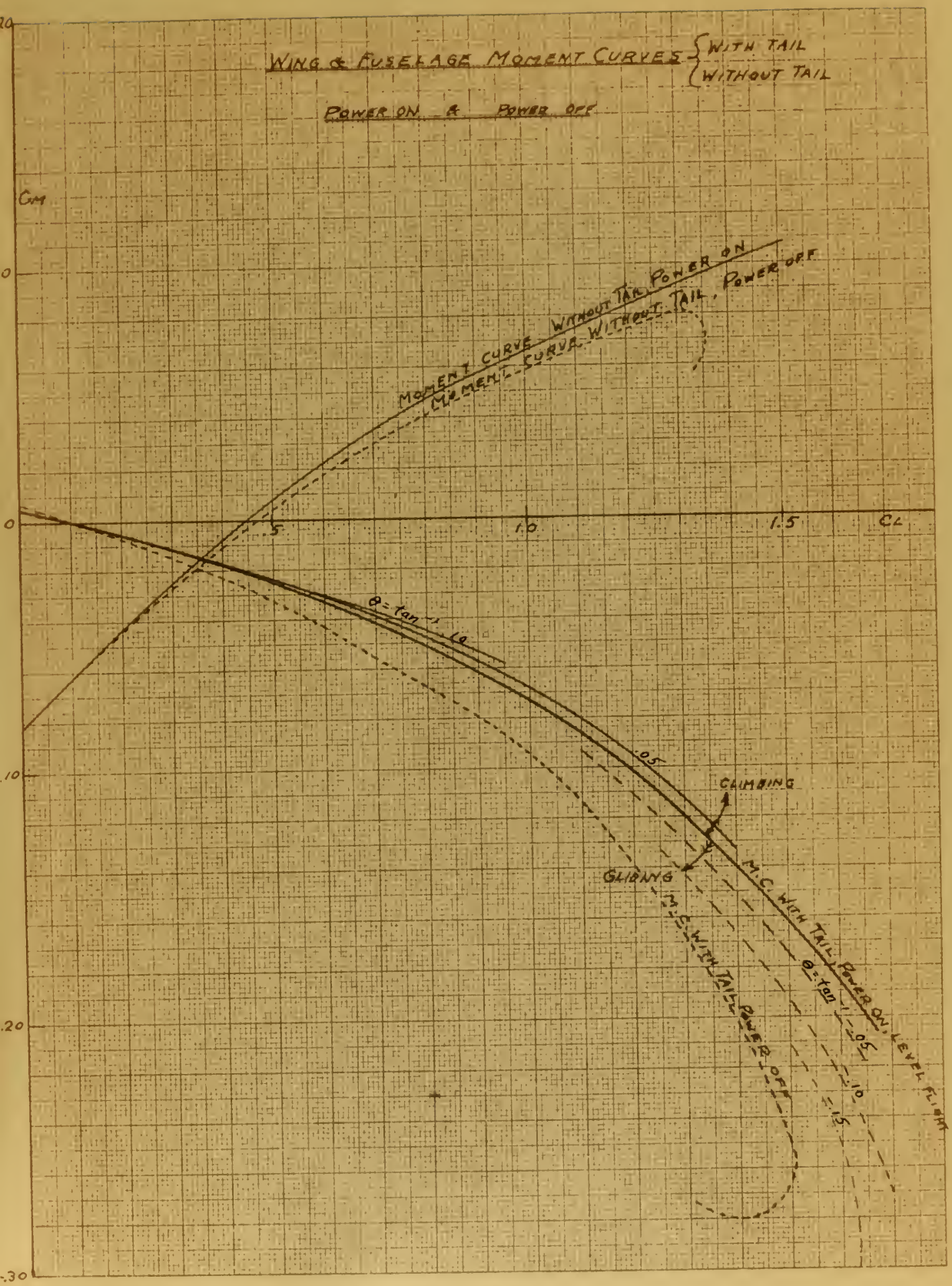
WING & FUSELAGE MOMENT CURVES { WITH TAIL / WITHOUT TAIL
POWER ON & POWER OFF
Cm
.20
0
.10
0
.5
1.0
1.5
CL
MOMENT CURVE WITHOUT TAIL, POWER ON
MOMENT CURVE WITHOUT TAIL, POWER OFF
θ = tan⁻¹ L/D
.05
CLIMBING
GLIDING
M.C. WITH TAIL POWER ON, LEVEL FLIGHT
M.C. WITH TAIL POWER OFF
θ = tan⁻¹ .05
.10
.15
.20
.30

FIGURE 23

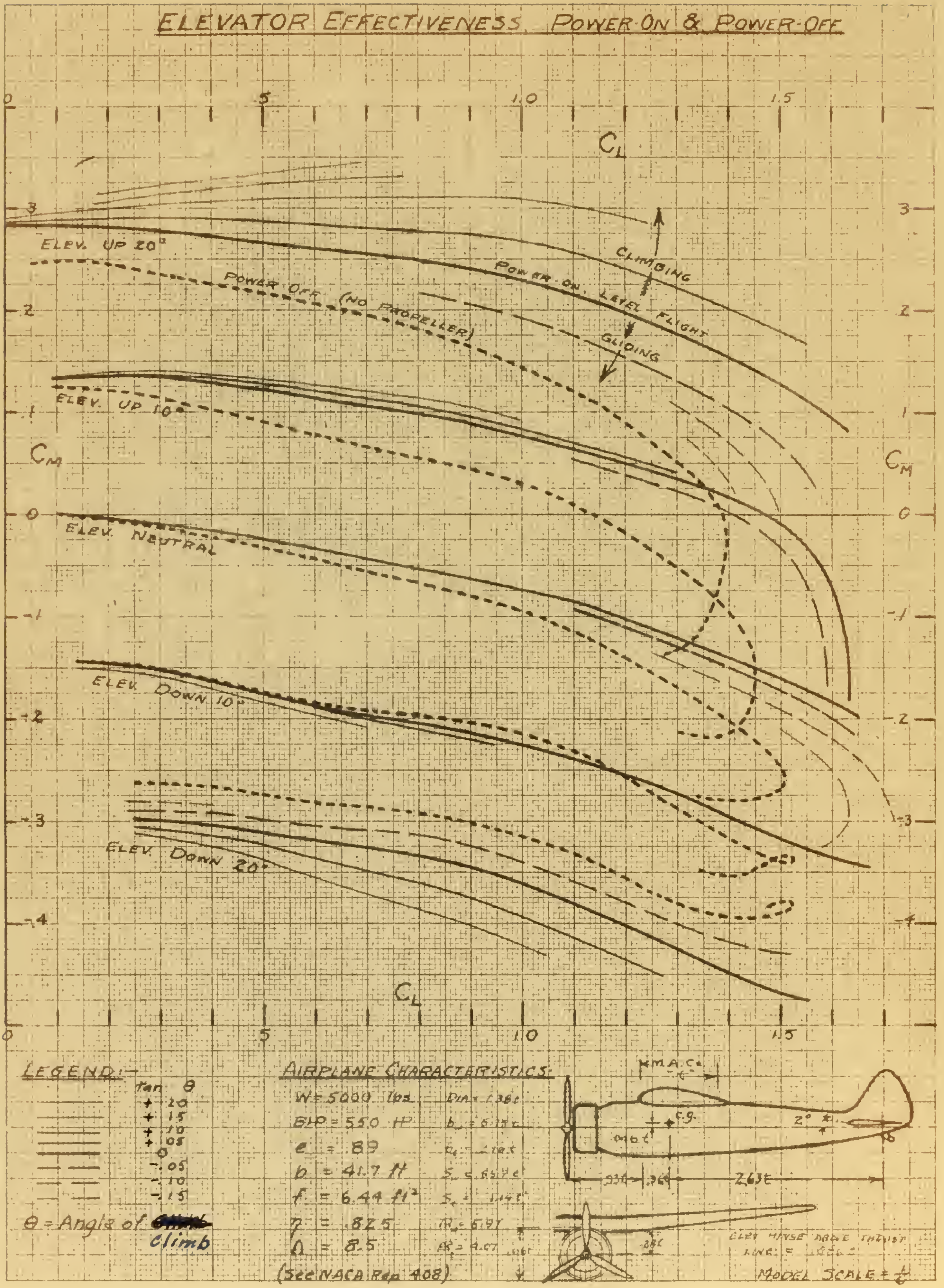
ELEVATOR EFFECTIVENESS, POWER-ON & POWER-OFF
C_L
C_M
ELEV. UP 20°
CLIMBING
POWER-ON, LEVEL FLIGHT
POWER-OFF (NO PROPELLER)
GLIDING
ELEV. UP 10°
ELEV. NEUTRAL
ELEV. DOWN 10°
ELEV. DOWN 20°
LEGEND:-
Tan θ
+ .20
+ .15
+ .10
+ .05
0
-.05
-.10
-.15
θ = Angle of Climb
AIRPLANE CHARACTERISTICS:
W = 5000 lbs.
BHP = 550 HP
e = .89
b = 41.7 ft
f = 6.44 ft²
η = .825
Λ = 8.5
(See NACA Rep. 408)
M.A.C.
C.G.
2°
MODEL SCALE = 1/6

FIGURE 24

presence of the slipstream.

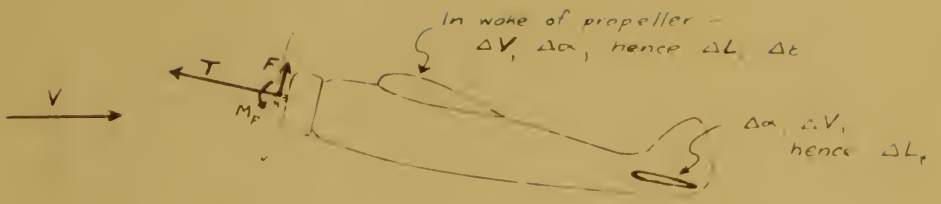

The addition of the operating propeller to an airplane in flight introduces forces and moments as shown in the sketch.

The normal force, "F", is caused by the angle of pitch. It exists whenever the propeller is delivering (or absorbing) torque and when the thrust axis and the velocity vector of air through the propeller are not coincident. It has been evaluated in various British "Reports and Memoranda", and the evaluations have been clearly summarized by Mr. C. H. Milliken in one memo. is appended to this report. "F" is a relatively small force but in this type of airplane acts at a relatively large distance from the center of gravity, hence may exert considerable moment in pitch.

Thrust, T, is a large force but acts at a small distance from the center of gravity. The aerodynamic moment of the propeller, M_F, is small and transfers directly to the center of gravity.

We have an accelerated flow over the center section of the wing and a change in the effective angle of attack. Hence the lift distribution and the downwash must change.

Now this accelerated and redirected flow arrives at the tail surfaces a change in lift of the tail result. Upon the lift at the tail surfaces, is normally depended for proper longitudinal

stability.

Nothing thus far has been said of the rotating character of the flow behind the propeller. Unfortunately difficulties in technique and lack of time prevented an investigation in this direction.

An effort was made to unearth some satisfactory method of predicting the slipstream effect on longitudinal static stability.

The technical staff of the Curtiss Company some years ago combined contemporary theory and some empirical propeller formulae, in order to express the change in angle of attack at the tail surface for various power conditions. Knowing the change in effective angle of attack at the tail and the increase in velocity due to slipstream, the change in lift on the horizontal surface can be estimated and hence the change in pitching moment. (See Curtiss Report #2721 "Slipstream Effect on Wings and Tailplane", Wm. H. Miller).

In applying this method, some assumption as to the portion of the horizontal tail surfaces effectively within the slipstream should certainly be incorporated. Estimated changes in moment by this method when applied to the model tests of this report showed a rather generous margin of conservatism.

A second method suggests itself. A tail effectiveness analysis such as that given by Dr. C. B. Millikan in his course in Aerodynamics of the Airplane, can be used with an arbitrary correction to the tail efficiency factor, η_t, to allow for slipstream. The arbitrary correction can be found by reference to standard tests,

power-on, in the wind tunnel for the type of plane under test. This appears a very approximate method of correcting for slipstream effect, but it can be used to give the designer at least some idea of the truth.

The method of tail moment estimation may be summarized as follows:

Consider the difference of angle of attack for zero lift of tail and wing.

α_d = ∠ between $C_L = 0$ for wing alone and $C_L = 0$ for tail alone.

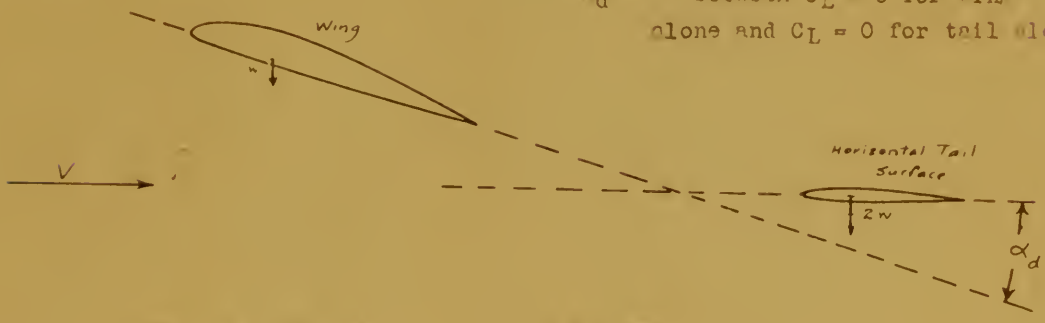

$\alpha_w = \alpha_t + \alpha_d = i_w$ $\qquad \alpha_t = \alpha_w - \alpha_d$

$\varepsilon_t = \dfrac{C_{L_t}}{\pi \, AR_t}$ = downwash at tail due to tail.

ε = downwash at tail due to wing

$\varepsilon_w = \dfrac{C_L}{\pi \, AR}$ = downwash at wing due to wing

Now the effective angle of attack of the tail is its geometrical angle of attack from zero lift minus downwash due to its own finite AR and minus downwash due to the wing operating ahead of it. This last we assume in practice to be twice the downwash of the wing at the wing. [illegible] the slope of the lift curve for tail if C_{L_t} may be considered as a practical constant for all normal angles.

Then C_{L_t} = a_o x effective angle of att ck of the tail

$$= a_o(\alpha_t - \varepsilon - \varepsilon_t)$$

$$= a_o (\alpha - \varepsilon_w - \varepsilon_w - \varepsilon_t - i_d) \quad \text{by the underlined assumption above.}$$

$$C_{L_t} = a_o\alpha_o - a_o \frac{C_L}{\pi AR} - a_o \frac{C_{L_t}}{\pi AR_t} - a_o\alpha_d$$

Assuming elliptic lift distribution for wing and tail surface

$$C_{L_t} + \frac{a_o}{\pi AR_t} C_{L_t} = C_L - \frac{a_o}{\pi AR} C_L - a_o\alpha_d$$

$$C_{L_t} = \frac{1 - \frac{a_o}{\pi AR}}{1 + \frac{a_o}{\pi AR_t}} C_L - \frac{a_o}{1 + \frac{a_o}{\pi AR_t}} \alpha_d$$

Now the pitching moment of the complete airplane is made up of that of tail and of another term primarily that of wing and fuselage but including all other factors.

$$M = M_{WF} + M_t = M_{WF} - L_t \ell \qquad \text{where } \ell = \text{tail length}$$

$$C_M = C_{WF} + C_{M_t} \qquad \text{where } C_{M_t} = \frac{M_t}{\frac{\rho V^2}{2} S_t} = - \frac{V_t^2}{V^2} \frac{\ell}{t} \frac{S_t}{S} C_{L_t}$$

Using C_{L_t} above

$$C_{M_t} = - \frac{V_t^2}{V^2} \frac{\ell}{t} \frac{S_t}{S} \left[\frac{1 - \frac{a_o}{AR}}{1 + \frac{a_o}{AR_{L_t}}} C_L - \frac{a_o}{1 + \frac{a_o}{AR_t}} \alpha_d \right]$$

But write

$$C_{M_t} = - \eta_t \frac{\ell}{t} \frac{S_t}{S} \left[\quad " \quad " \quad \right]$$

and η_t will account for effective velocity at the tail, and other errors such as that of the assumption of wing downwash at the tail.

It will be noted that the term contained in the expression derived above for pitching moment due to tail is controlled by the pilot with a stabilizer or trimming tab adjustment, but that the multiplicative factors, — the tail volume coefficient, $\frac{l S_t}{t S}$, and, within narrow limits, tail efficiency, η_t, — are controlled by the designer.

Differentiating the tail moment expression with respect to C_L we get:

$$\frac{dC_{M_t}}{dC_L} = -\eta_t \frac{l S_t}{t S} \left[\frac{1 - \frac{a_o}{\pi AR}}{1 + \frac{a_o}{\pi AR_t}} \right]$$

η_t can then be determined by graphical solution on C_M vs. C_L curves for any operating range desired. This can be done for the ordinary wind tunnel model without propeller and then an appropriate correction applied for power-on for the type of plane and position of tail. The correction can be estimated by reference to power-on tests of models of similar type.

In our experiment the slopes of the tail moment curves against C_L for various conditions were determined graphically, and the tail efficiencies computed. For our model

$$\frac{dC_{M_t}}{dC_L} = -\eta_t \frac{22^{2} \times 60.2}{[illegible]} \left[\frac{1 - 5.5/5.97}{1 + 5./4.07} \right] = -.226\ \eta_t$$

$$\text{or } \eta_t = \frac{-dC_{M_t}/dC_L}{.266}$$

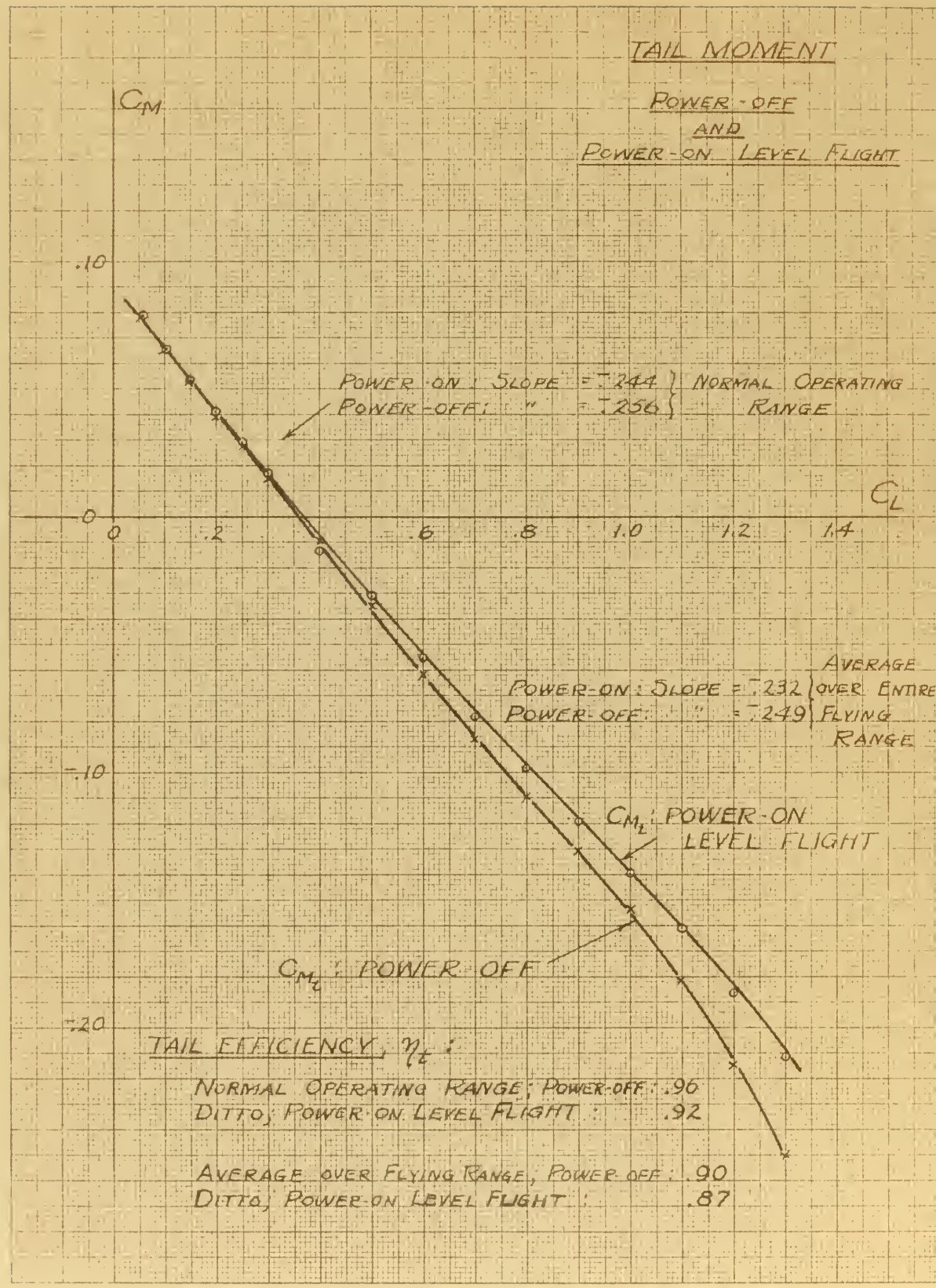

FIGURE 25

p 291

Condition	$-\frac{dC_{m_t}}{dC_L}$	η_t	$\Delta\eta_t$
Power-on, C_L range for normal flight	.244	.916	-.046
Power-off, " " " " "	.256	.962	
Power-on, entire range of C_L, mean value,	.232	.872	-.026
Power-off, " " " " " " ,	.249	.898	

Hence if η_t were determined from an ordinary wind tunnel model of the airplane type used in this experiment, it should be reduced 0.04 in order to approximate power-on effectiveness.

A comparison of the individual contributions of the wing and fuselage as a unit, and of the tail, to the destabilized condition, power-on, is of interest.

$$C_m = C_{m_{WF}} + C_{m_t}$$

$$\frac{dC_m}{dC_L} = \frac{dC_{m_{WF}}}{dC_L} + \frac{dC_{m_t}}{dC_L}$$

Power-on	-.059	= .185	-	.244
Power-off	-.086	= .170	-	.256
Change	.027	= .015	+	.012

which indicates that the wing and fuselage, and the tail, have shared almost equally in reducing the longitudinal static stability.

The writers feel that in this research problem of power effects on a high wing monoplane, the field of power-on investigation has been barely touched. The model used can be readily converted to low wing, and there is, in process of manufacture, a tail on which the horizontal surface can be displaced vertically as well as having

adjustable stabilizer incidence, elevator angle, and tab angle. It is hoped that the next class of graduate students in aeronautics at the California Institute of Technology will be able to extend the glimpse we have had of power effects on the airplane.

Grateful acknowledgment is made to the staff of assistants in the wind tunnel, to Dr. A. L. Klein for his able design of our apparatus, to Dr. C. B. Millikan for his direction of our research schedule and valuable assistance with many knotty problems, and to the head of the Department of Aeronautics, Dr. Theodor von Karman, for his inspiring interest and clarifying suggestions.

TABLE OF NOTATION

A_W = aspect ratio of wing

A_t = aspect ratio of tail surfaces

C_D = drag coefficient = $\frac{D}{qS}$

C_{D_θ} = drag coefficient, power-on, defined as in text

C_L = lift coefficient = $\frac{L}{qS}$

C_m = pitching moment coefficient = $\frac{M}{qtS}$

C_R = coefficient of resultant force dragwise, power-on = $\frac{R}{qS}$

C_{Q_S} = torque speed coefficient

C_T = thrust coefficient = $\frac{T}{\rho n^2 D^4}$

C_Q = torque coefficient = $\frac{Q}{\rho n^2 D^5}$

C_s = speed power coefficient = $\frac{\rho^{1/5} V}{n^{2/5} P^{1/5}}$

c = velocity of sound

D = propeller diameter

D = drag, force in direction of air velocity

D_p = parasite drag

D_o = drag, force power-off and $C_L = 0$

D_θ = drag, force power-on, defined as in text

e = airplane efficiency factor

f = equivalent parasite area*

F = force developed by a propeller normal to its axis of rotation

h = altitude above sea-level

J = propeller advance ratio = $\frac{V}{n D}$

k = a constant

L = lift, force normal to air velocity

ℓ = tail length, c.g. to elevator hinge

l_p = parasite loading performance parameter = $\frac{W}{f}$ *

l_s = span loading performance parameter = $\frac{W}{e(\pi b)^2}$ *

l_t = weight thrust power parameter = $\frac{W}{bhp_m \eta_o}$ *

l_w = wing loading = $\frac{W}{S}$

M = pitching moment of model about c.g.

M_p = pitching moment of propeller about intersection of its axis of rotation and plane of the blades

N = revolutions per minute

n = revolutions per second

P = power (normally brake horsepower)

Q = torque developed in propeller shaft

C_c = torque coefficient = $\frac{Q}{\rho V^2 D^3} = \frac{Q}{2qD^3}$

R_J = ratio J to design J

R_N = ratio N to design maximum N

R_V = ratio V to design maximum V

q = dynamic pressure = $\frac{\rho V^2}{2}$

R = resultant dragwise force, power-on

S = wing area

t = chord length

T = thrust

T_e = effective thrust

Thp_a = thrust horsepower available

Thp_r = thrust horsepower required

V = air velocity

V_s = air velocity in slipstream

W = weight of airplane

w = downwash velocity

α = angle of attack (measured from thrust axis in this experiment)

β = blade angle of propeller

Δ indicates "increment in"

δ = total linear deflection

ε = downwash angle

η = propulsive efficiency = $\frac{T_e V}{P}$ at $\alpha = 0$

η' = propulsive efficiency at α's other than zero

η_t = tail efficiency

γ = angle of climb (negative values indicate glide)

Λ = airplane performance parameter*

ρ = air density

σ = air density relative to standard density at sea-level = ρ/ρ_o

ϕ = total angular deflection

$\backsim$ = "corresponds to"

$\supset$ = "implies and is implied by"

$\angle$ = "angle"

---

*cf. '. . . . Technical Report 408.

SIDE FORCE ON A YAWED PROPELLER*

Appendix by C. B. Millikan

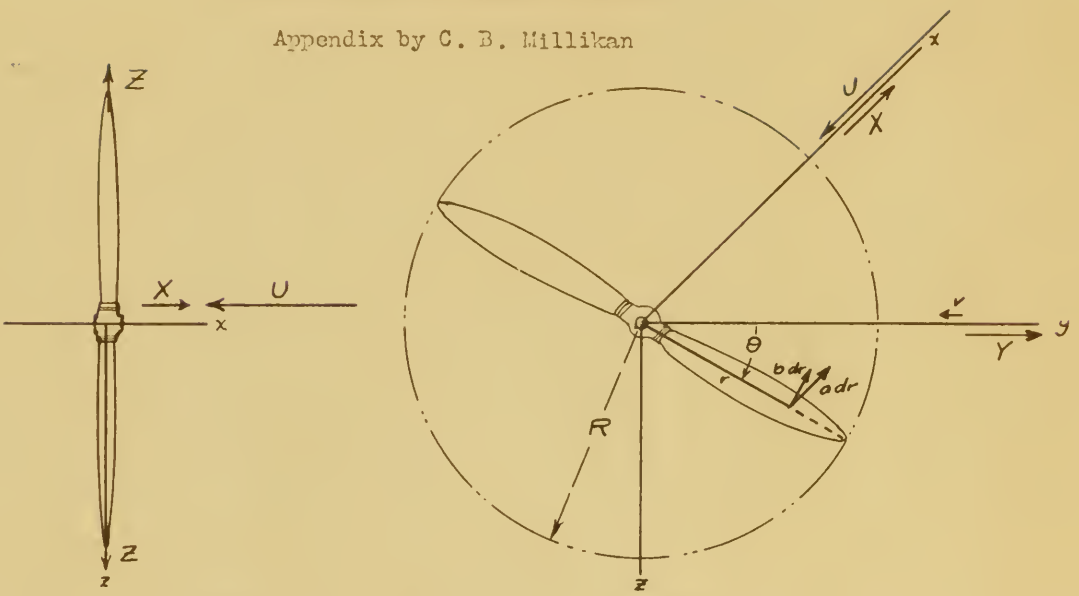

Let a = thrust loading per unit length of span along a blade

b = torque force loading per unit length of span along a blade

adr = thrust on a blade element dr

rbdr = torque on a blade element dr

X,Y,Z = forces on propeller

X = thrust, Y = side force

The relative wind striking the propeller has components U, v.

In general v $\ll$ V, i.e. we consider small angles of yaw.

---

* cf. H. G. Harris "Forces on a Propeller Due to Sideslip", R & M No. 427; and M. Glauert "The Stability Derivatives of an Airscrew", R & M No. 642.

At a given instant let θ define the position of a propeller blade. Σ indicates summation over all (B) propeller blades.

1) $$X = \sum_B \int_0^R a\,dr \quad ; \quad Y = \sum_B \int_0^R \sin\theta\, dr$$

Consider the propeller acting in a purely axial velocity U and at a given $J = \frac{U}{nD}$. Then the equilibrium conditions are:

$$Y = Y_0 = 0, \text{ and } X = X_0$$

We ask for the changed X,Y due to a side wind v. If v is small, we assume

2) $$X = X_0 + \frac{\partial X}{\partial v} v = X_0 + X_v v$$

$$Y = Y_0 + \frac{\partial Y}{\partial v} v = vY_v$$

Now a and b are proportional to the local u^2 (u = circumferential velocity) and to a function of the local $J = J'$, i.e. $a,b \backsim u^2 f(J)$ where

$$J' = \frac{U}{2\pi r} = \frac{\pi U}{u}$$

Write $a = ku^2 f(J')$. Let δ correspond to an increment at a given blade element due to a change in conditions at the element.

$$\delta a = ku^2 \cdot f(J') \cdot \frac{2\delta u}{u} + ku^2 f \frac{\partial f}{\partial J'} \frac{\delta f}{f}$$

$$= a \cdot 2\frac{\delta u}{u} + \frac{\partial a}{\partial J'} \delta J'$$

$$\therefore \quad \delta a = 2\left(a \frac{\delta u}{u} \quad \frac{1}{2} \quad \frac{\partial a}{\partial J'} \delta J'\right)$$

$$\delta b \qquad 2\left(b \frac{\delta u}{u} \quad \frac{1}{2} \quad \frac{\partial b}{\partial J'} \delta J'\right)$$

But $J' = \frac{\pi U}{u}$ $\quad \therefore \quad \delta J' = -\frac{\pi U}{u} \quad \frac{\delta u}{u} = -J' \quad \frac{\delta u}{u}$

$$\therefore \quad \delta a = 2 \frac{\delta u}{u} \left(a - \frac{J'}{2} \frac{\partial a}{\partial J'}\right)$$

$$\delta b = 2 \frac{\delta u}{u} \left(b - \frac{J'}{2} \frac{\partial b}{\partial J'}\right)$$

and $u = 2 \pi nr$, $\quad \delta u = -v \sin \theta \quad \therefore \quad \frac{\delta u}{u} = -\frac{v \sin \theta}{2 \pi nr}$

$$\therefore \qquad \delta a = -\frac{v \sin \theta}{nr} \Delta a$$

3) $$\delta b = -\frac{v \sin \theta}{nr} \Delta b$$

$$\Delta ( ) = \left(1 - \frac{J}{2} \frac{\partial}{\partial J}\right) ( ) \qquad J = \frac{U}{n(2R)}$$

Here we have replaced the local $J' = \frac{U}{2 \pi nr}$ by $J = \frac{U}{2 \pi nR}$ (or $\frac{V}{nD}$).

This is justified by the following argument:

$$J \frac{\partial f(r)}{\partial J} = \frac{U}{nR} \frac{\partial f}{\partial \frac{U}{nR}}$$

$$J' \frac{\partial f(r)}{\partial J'} = \frac{U}{nr} \frac{\partial f}{\partial \frac{U}{nr}}$$

Now consider a given blade element, i.e. r = const. Then we get the variation in f by varying $\frac{V}{n}$ keeping r constant

$$\therefore \quad J \frac{\partial f}{\partial J} = \frac{V}{n} \frac{\partial f}{\partial \frac{V}{n}} = J' \frac{\partial f}{\partial J'}$$

But our partial derivative in Δ means just this, i.e. we consider the variation in force on a given blade element as the aerodynamic conditions change.

$$\therefore J' \frac{\partial}{\partial J'} = J \frac{\partial}{\partial J} \qquad \therefore \quad \Delta \text{ is independent of r.}$$

Now

$$\delta X = v X_v = \delta \sum_B \int_o^R a\,dr = \sum_B \int_o^R \delta a\,dr$$

$$\delta Y = \sum_B \int_o^R \delta b \sin\theta\,dr$$

Here the integration and variation are interchangeable since the expressions are linear in a and b.

$$\therefore \delta X = \sum_B -\frac{v \sin\theta}{\pi n} \int_o^R \Delta\, a \frac{dr}{r}$$

$$\delta Y = \sum_B -\frac{v \sin^2\theta}{n} \int_o^R \Delta\, b \frac{dr}{r}.$$

Now since Δ is independent of r we may interchange its position with that of the integral sign. We are interested only in the average force which means we must integrate over θ from $0 \longrightarrow 2\pi$ and divide by 2π. This will give the average force per blade.

For the whole propeller we must multiply by the number of blades, B.

This gives

$$\delta X = 0$$

4)
$$\delta Y = -\frac{Bv}{2\pi n} \Delta \int_0^R b \frac{dr}{r}$$

Hence the thrust due to side-slip is zero for small side-slips.

In discussing the integral in 4) it is convenient to define a dimensionless torque loading factor β :

$$\beta = B \frac{bR^2}{Q} \qquad \therefore \quad Bb = \beta \frac{Q}{R^2}$$

$$\therefore Q = B \int_0^R brdr = Q \int_0^R \beta \frac{rdr}{R^2}$$

5)
$$\beta = B \frac{bR^2}{Q} \quad , \quad \xi = \frac{r}{R} \qquad \therefore \int_0^1 \beta \xi \, d\xi = 1$$

$$\delta Y = -\frac{v}{2\pi nR^2} \Delta Q \int_0^R \frac{\beta \, dr}{r}$$

$$\delta Y = \frac{-v}{2\pi nR^2} \Delta Q \int_0^1 \beta \frac{d\xi}{\xi}$$

Now, in the R & M's (loc. cit), it is assumed that

6)
$$\int_0^1 \beta \frac{d\xi}{\xi} = K = \text{universal constant independent of J,}$$

i.e. all torque grading curves for all propellers are similar and have

a shape independent of J.

$$\therefore \quad \delta Y = -\frac{v\,k\,\Delta Q}{\frac{\pi}{2}nD^2} = \frac{-2kJ}{\pi VD}\left(Q_c - \frac{J}{2}\frac{dQ}{dJ}\right)v$$

$$= -\frac{2kQJ}{\pi vD}\left(1 - \frac{J}{2Q_c}\frac{dQ_c}{dJ}\right)v$$

$$\therefore \quad \delta Y = -\frac{2k}{\pi}\frac{QJ}{D}(1 - \lambda_Q)\cdot v'U$$

7) $\lambda_Q = \frac{1}{2}\frac{J}{Q_c}\frac{dQ_c}{dJ}$ $\qquad k = 1.6$ From R. & M. 642

Q_c = torque coefficient

Determination of k

In R. & M. 607 it is assumed:

$$0 \le \xi \le \xi_1 \;\therefore\; \beta = 0 \quad ; \qquad \xi_1 \le \xi \le 1 \;\therefore\; \beta = \beta_0$$

$$\therefore k = \beta_0 \int_{\xi_1}^{1} \frac{d\xi}{\xi} = \beta_0 \log \frac{1}{\xi_1}$$

But $\int_0^1 \beta\,\xi\,d\xi = 1 \qquad \therefore \beta_0 \frac{\xi^2}{2}\Big]_{\xi_1}^{1} = 1 \qquad \therefore \beta_0 = \frac{2}{1-\xi_1^2}$

$$\therefore k = \frac{2}{1-\xi_1^2}\log\frac{1}{\xi_1}$$

ξ_1 is taken as .175 $\therefore \frac{2}{1-\xi_1^2} = 2.06 \quad \therefore k = 2.06 \log_e 5.72 = 2.06 \times 1.745 = 3.6$

Hence the side force F on a propeller inclined at angle θ to the airflow

is

$$F = \frac{2k}{\pi}\frac{QJ}{D}(1 - \lambda_Q) \cdot \theta$$

8)

$$\lambda_Q = \frac{1}{2}\frac{J}{Q_c}\frac{dQ_c}{dJ}$$

$\overline{F}$ is in the same direction as the side vector $\overline{v}$.

In R. & M. 642, it is assumed that

9)

$$Q_c = A_Q(a - \lambda^3)$$

$$T_c = A_T(1 - \lambda^2)$$

where $\lambda = J/J_o$; $J_o \sim T_c = 0$, i.e. J for zero thrust

$$\therefore \lambda_Q = \frac{1}{2}\frac{\lambda A_Q(-3\lambda^2)}{A_Q(a - \lambda^3)} = -\frac{3}{2}\frac{\lambda^3}{a - \lambda^3}$$

$$\therefore F = \frac{2k}{\pi}\frac{QJ}{D}\left(1 + \frac{3}{2}\frac{\lambda^3}{a - \lambda^3}\right) \cdot \theta$$

But $\eta = \frac{TU}{2\pi nQ}$ $\quad\therefore Q = \frac{TU}{2\pi n\eta}$

$$\therefore F = \frac{2k}{\pi}\frac{TJ^2}{2\pi\eta}\frac{a + \frac{1}{2}\lambda^3}{a - \lambda^3}\theta$$

$$\therefore \frac{F}{T} = \frac{k}{2\pi^2}\frac{J_o^2}{\eta m}\frac{2(2a + \lambda^3)}{m(a - \lambda^3)}\theta$$

$m = \eta/\eta_m$, $\lambda = J/J_o$, $a = 1.325$, $k = 3.6$

The numerical values for a and k are those given in the N. & M.'s. We have already discussed the numerical value of k. Consider a

$$\frac{J(Q = 0)}{J(T = 0)} = a^{\frac{1}{3}}$$

Hence a = 1.325 corresponds to the assumption

$$\frac{J(Q = 0)}{J(T = 0)} = (1.325)^{\frac{1}{3}} = 1.1$$

In Fig. 26 are plotted quadratic and cubic approximations to C_T and C_Q. It is seen that these approximations may be determined so as to fit the experimental points very well indeed. However, we have here

$$\frac{J(Q = 0)}{J(T = 0)} = 1.040 \quad \text{i.e.}$$

$$a = 1.12$$

From CALCIT measurements 3 bladed propeller; $\beta = 30.3°$.

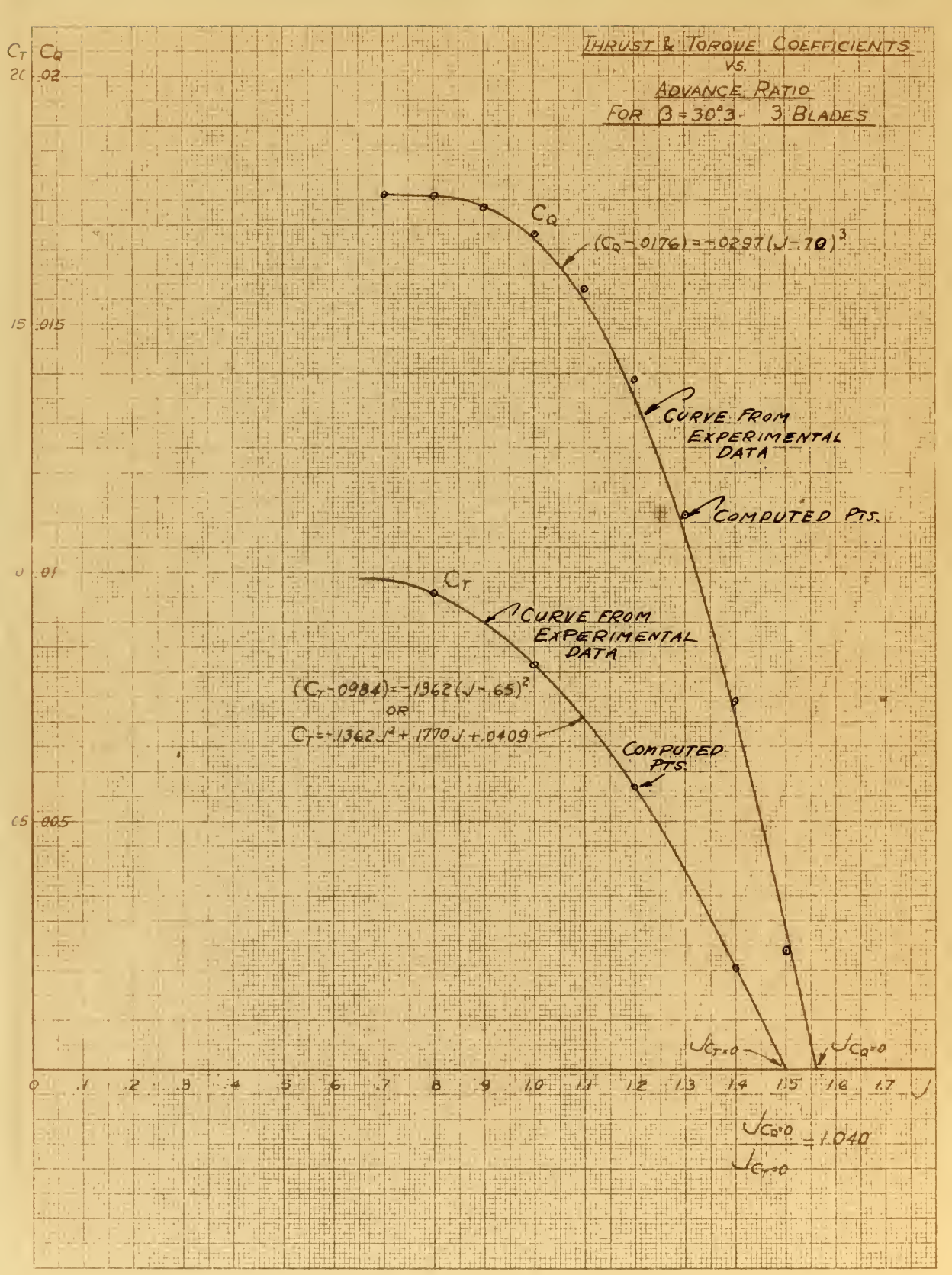
C_T C_Q
.02
.015
.01
.005
THRUST & TORQUE COEFFICIENTS
VS.
ADVANCE RATIO
FOR β = 30°3' 3 BLADES
C_Q
$(C_Q - .0176) = -.0297 (J - .70)^3$
CURVE FROM EXPERIMENTAL DATA
COMPUTED PTS.
C_T
CURVE FROM EXPERIMENTAL DATA
$(C_T - .0984) = -.1362 (J - .65)^2$
OR
$C_T = -.1362 J^2 + .1770 J + .0409$
COMPUTED PTS.
$J_{C_T=0}$
$J_{C_Q=0}$
0 .1 .2 .3 .4 .5 .6 .7 .8 .9 1.0 1.1 1.2 1.3 1.4 1.5 1.6 1.7 J
$\frac{J_{C_Q=0}}{J_{C_T=0}} = 1.040$

FIGURE 26

Thesis 6304
R9 Russell
Propeller characteristics and slipstream effects on a high wing monoplane from wind tunnel tests.

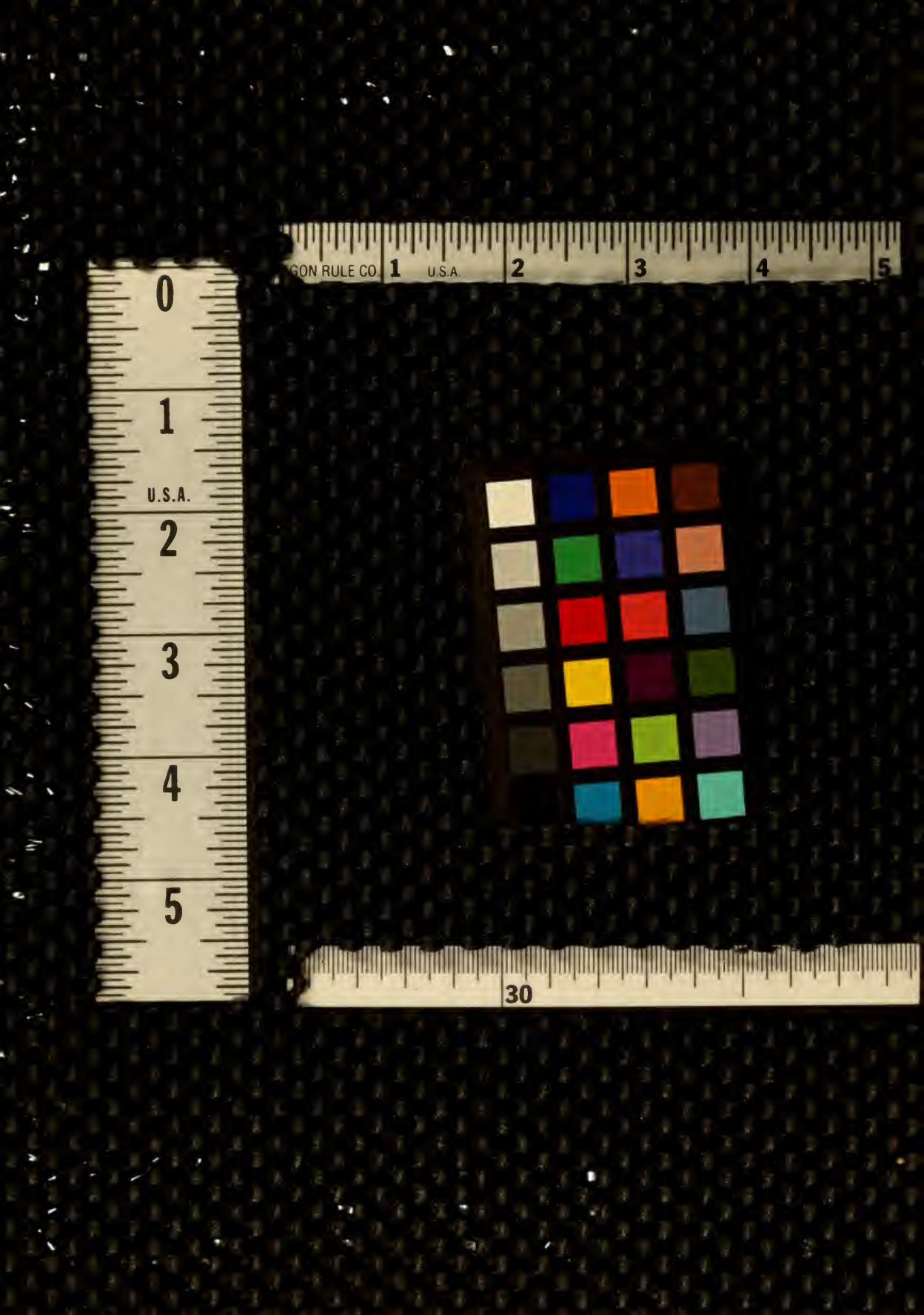
GON RULE CO.
1
U.S.A.
2
3
4
5
0
1
U.S.A.
2
3
4
5
30